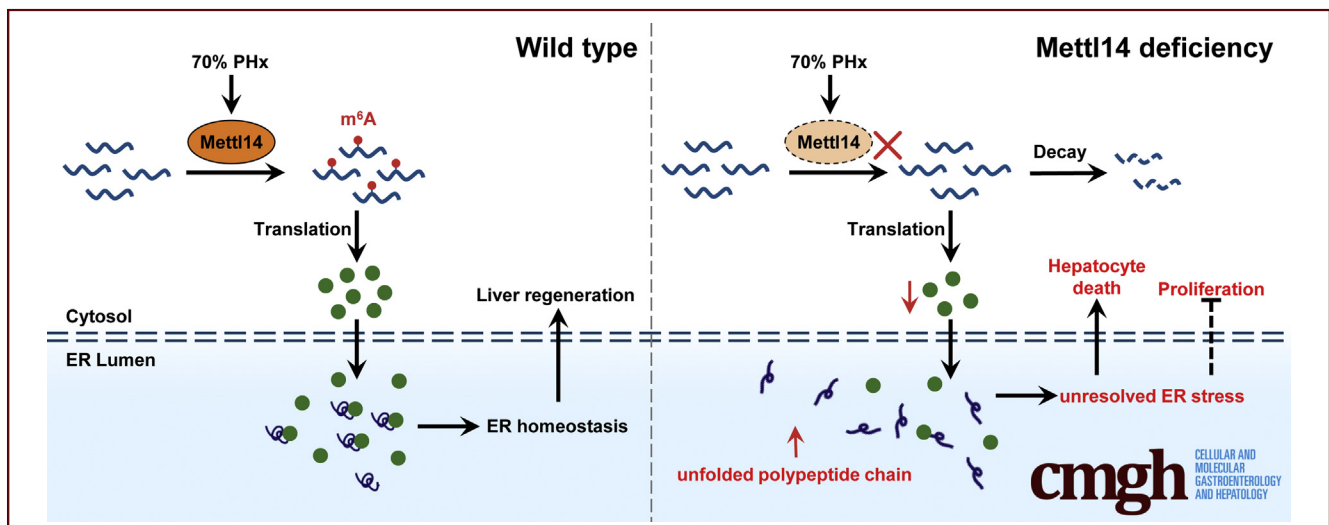


## ORIGINAL RESEARCH

Mettl14-Mediated m<sup>6</sup>A Modification Facilitates Liver Regeneration by Maintaining Endoplasmic Reticulum Homeostasis

Xiaoyue Cao,<sup>1</sup> Yuke Shu,<sup>1</sup> Yuwei Chen,<sup>1</sup> Qing Xu,<sup>1</sup> Gang Guo,<sup>2</sup> Zhenru Wu,<sup>1</sup> Mingyang Shao,<sup>1</sup> Yongjie Zhou,<sup>1</sup> Menglin Chen,<sup>1</sup> Yuping Gong,<sup>3</sup> Chuan Li,<sup>4</sup> Yujun Shi,<sup>1</sup> and Hong Bu<sup>1,5</sup>

<sup>1</sup>Laboratory of Pathology, Key Laboratory of Transplant Engineering and Immunology, NHC, West China Hospital, Sichuan University, Chengdu; <sup>2</sup>Department of Talent Highland, Center for Gut Microbiome Research, First Affiliated Hospital of Xi'an Jiao Tong University, Xian; <sup>3</sup>Department of Hematology, West China Hospital, Sichuan University, Chengdu; <sup>4</sup>Department of Liver Surgery, West China Hospital, Sichuan University, Chengdu; and <sup>5</sup>Department of Pathology, West China Hospital, Sichuan University, Chengdu, China



## SUMMARY

The N<sup>6</sup>-methyladenosine (m<sup>6</sup>A) methyltransferase Mettl14 promotes polypeptide-processing protein expression in an m<sup>6</sup>A-dependent manner, and loss of Mettl14 in vivo leads to excessive ER stress, resulting in impaired liver regeneration.

**BACKGROUND & AIMS:** N<sup>6</sup>-methyladenosine (m<sup>6</sup>A), the most prevalent and dynamic posttranscriptional methylation modification of mammalian mRNA, is involved in various biological processes, but its role in liver regeneration has not been characterized.

**METHODS:** We first conducted transcriptome-wide m<sup>6</sup>A mRNA sequencing and characterized the expression pattern of m<sup>6</sup>A in regenerating mouse liver. Next, we generated hepatocyte-specific Mettl3- or Mettl14-deficient mice and investigated their role in liver regeneration. A series of biochemical experiments in vitro and in vivo was further performed to investigate potential mechanisms.

**RESULTS:** We identified an overwhelming proportion of m<sup>6</sup>A-modified genes with initially up-regulated and subsequently down-regulated m<sup>6</sup>A levels as liver regeneration progressed. Loss of Mettl14 but not of Mettl3 resulted in markedly disrupted liver regeneration, and Mettl14-ablated hepatocytes were arrested in the G1 phase of the cell cycle. Most strikingly, the Mettl14-ablated regenerating liver exhibited extensive parenchymal necrosis. mRNA transcripts, such as *Hsp90b1*, *Erp29*, *Stt3a*, *P4hb*, and *Lman1*, encoding proteins involved in polypeptide processing and the endoplasmic reticulum (ER) stress response, were m<sup>6</sup>A-hypomethylated, and their mRNA and protein levels were subsequently decreased, resulting in unresolved ER stress, hepatocyte death, and inhibited proliferation.

**CONCLUSIONS:** We demonstrate the essential role of Mettl14 in facilitating liver regeneration by modulating polypeptide-processing proteins in the ER in an m<sup>6</sup>A-dependent manner. (*Cell Mol Gastroenterol Hepatol* 2021;12:633–651; <https://doi.org/10.1016/j.jcmgh.2021.04.001>)

**Keywords:** Mettl14; N<sup>6</sup>-methyladenosine; Liver Regeneration; Endoplasmic Reticulum Stress.

The liver is one of the few solid organs with a high regeneration capacity. After partial hepatectomy (PHx) or chemical challenge in the mammalian liver, almost all remnant hepatocytes rapidly initiate mitosis to generate new cells, and the liver can be reconstituted within 1 week.<sup>1,2</sup> Many genes and signaling pathways are involved in this process. For example, immediately after PHx, approximately 100 immediate-early genes are activated to promote quiescent hepatocyte re-entry into the cell cycle.<sup>3,4</sup> Subsequently, active gene transcription and protein synthesis occur in proliferating cells until complete reconstitution of the liver mass and remodeling of the lobular structure. The whole liver regeneration process is precisely controlled by comprehensive genetic and epigenetic gene modulation, and any disturbances in these modulations can lead to abnormal liver regeneration and various liver diseases, such as liver failure, cirrhosis, and hepatocellular carcinoma (HCC).<sup>4,5</sup> Understanding the mechanism of liver regeneration has the potential to provide clues for better prevention and treatment of liver diseases.

N<sup>6</sup>-methyladenosine (m<sup>6</sup>A), the most prevalent methylation modification of mammalian mRNA,<sup>6</sup> participates in almost every stage of RNA metabolism, including RNA splicing, folding, transport, translation, and decay, and subsequently modulates the expression of many genes.<sup>7–11</sup> Methyltransferase-like 3 (Mettl3), Mettl14, and Wilms' tumor 1-associated protein (WTAP) are methyltransferases of m<sup>6</sup>A, also called m<sup>6</sup>A writers, and they assemble into a methyltransferase complex to install m<sup>6</sup>A on mRNA.<sup>6,12,13</sup> In contrast, fat mass and obesity-associated protein (FTO) and ALKB family member 5 protein (Alkbh5) act as erasers that remove m<sup>6</sup>A modifications.<sup>14,15</sup> The m<sup>6</sup>A writers and erasers coordinatively make the m<sup>6</sup>A modification dynamic and reversible. Dysregulation of either writers or erasers affects the m<sup>6</sup>A level, which then disrupts various biological behaviors. m<sup>6</sup>A is dynamically regulated during spermatogonia stem cell development, and either single or combined loss of Mettl3 and Mettl14 disturbs spermiogenesis.<sup>16</sup> Mutation of Mettl14 or down-regulation of Mettl3 disrupts the translation of the AKT negative regulator PHLPP2 and increases the expression of the positive AKT regulator mTORC2, therefore activating the AKT pathway and leading to endometrial cancer cell proliferation.<sup>17</sup> Interestingly, m<sup>6</sup>A can either promote or suppress target gene expression. Mettl14-mediated m<sup>6</sup>A destabilizes the mRNA stability of histone acetyltransferases to suppress histone modification in vivo and enhances the self-renewal of mouse embryonic neural stem cells.<sup>18</sup> In contrast, Mettl14-mediated m<sup>6</sup>A has a possible role in improving mRNA stability, because Mettl14 inhibition in acute myeloid leukemia decreases the mRNA stability and translation of MYC and MYB, resulting in a disruption of proliferation and increased apoptosis in cultured tumor cells.<sup>19</sup> m<sup>6</sup>A also plays a role in HCC. Mettl3 overexpression promotes liver cancer cell growth by reducing SOCS2 mRNA stability in an m<sup>6</sup>A-dependent manner.<sup>20</sup> In contrast,

Mettl14-mediated m<sup>6</sup>A acts as a tumor suppressor in HCC by interacting with DGCR8 to promote the maturation of tumor-suppressive microRNAs.<sup>21</sup> Mettl3 and Mettl14 may play different roles by targeting different genes, but further confirmation is required. Moreover, most of the knowledge is acquired from in vitro experiments and remains controversial. Furthermore, the role of m<sup>6</sup>A modification in liver regeneration, which involves rapid and dynamic regulation of a great number of genes, has not yet been reported.

Here we constructed a mouse model of liver regeneration and demonstrated that both Mettl3 and Mettl14 were rapidly increased and accompanied by significant elevation in global m<sup>6</sup>A modifications of mRNA after PHx. Liver-specific loss of Mettl14 but not that of Mettl3 significantly impaired liver regeneration and led to marked hepatocyte death. Mechanistically, the regenerating Mettl14-deficient hepatocytes exhibited excessive endoplasmic reticulum (ER) stress, which was at least partly due to the reduced expression of polypeptide-processing proteins in the ER in an m<sup>6</sup>A-dependent manner.

## Results

### *Dynamic m<sup>6</sup>A Modification During Liver Regeneration*

To elucidate the m<sup>6</sup>A expression pattern during liver regeneration, liver tissues were collected at the indicated times after 70% PHx in mice. Quantitative polymerase chain reaction (qPCR) and immunoblotting revealed that the levels of both m<sup>6</sup>A methyltransferases Mettl3 and Mettl14 markedly increased and rapidly reached their maximum levels at 3 and 6 hours after PHx, respectively. Then their levels began to decrease and returned to basal levels either quickly or slowly (Figure 1A and B). Correspondingly, colorimetric analysis showed that the global m<sup>6</sup>A levels in the liver gradually increased with the progress of regeneration (Figure 1C). These findings suggest that by regulating m<sup>6</sup>A modification, Mettl3 and Mettl14 may positively contribute to liver regeneration.

**Abbreviations used in this paper:** Act D, actinomycin; Alkbh5, ALKB family member 5 protein; ALT, alanine aminotransferase; AMPK, adenosine 5'-monophosphate-activated protein kinase; AST, aspartate aminotransferase; ATF6, activating transcription factor 6; BrdU, 5-bromo-2-deoxyuridine; CDS, coding sequence; Chop, C/EBP-homologous protein; eIF2 $\alpha$ , eukaryotic translation initiator factor 2 $\alpha$ ; EIF3A, eukaryotic translation initiation factor 3 subunit A; ER, endoplasmic reticulum; ERK, extracellular signal-regulated kinase; FC, fold change; FoxM1, forkhead box M1; FTO, fat mass and obesity-associated protein; HCC, hepatocellular carcinoma; IRE1 $\alpha$ , inositol requiring enzyme 1 alpha; JAK, janus kinase; MAPK, mitogen-activated protein kinase; Mettl3, methyltransferase-like 3; m<sup>6</sup>A, N<sup>6</sup>-methyladenosine; m<sup>6</sup>A-seq, m<sup>6</sup>A sequencing; PAS, periodic acid-Schiff; PERK, protein kinase R-like endoplasmic reticulum kinase; PHx, partial hepatectomy; PI3K, phosphatidylinositol 3-kinase; qPCR, quantitative polymerase chain reaction; STAT, signal transducers and activators of transcription; TM, tunicamycin; TUDCA, tauroursodeoxycholate; UPR, unfolded protein response; UTR, untranslated region; WT, wild-type; WTAP, Wilms' tumor 1-associated protein; XBP1, X-box-binding protein 1.



Most current article

© 2021 The Authors. Published by Elsevier Inc. on behalf of the AGA Institute. This is an open access article under the CC BY-NC-ND license (<http://creativecommons.org/licenses/by-nc-nd/4.0/>).

2352-345X

<https://doi.org/10.1016/j.jcmgh.2021.04.001>

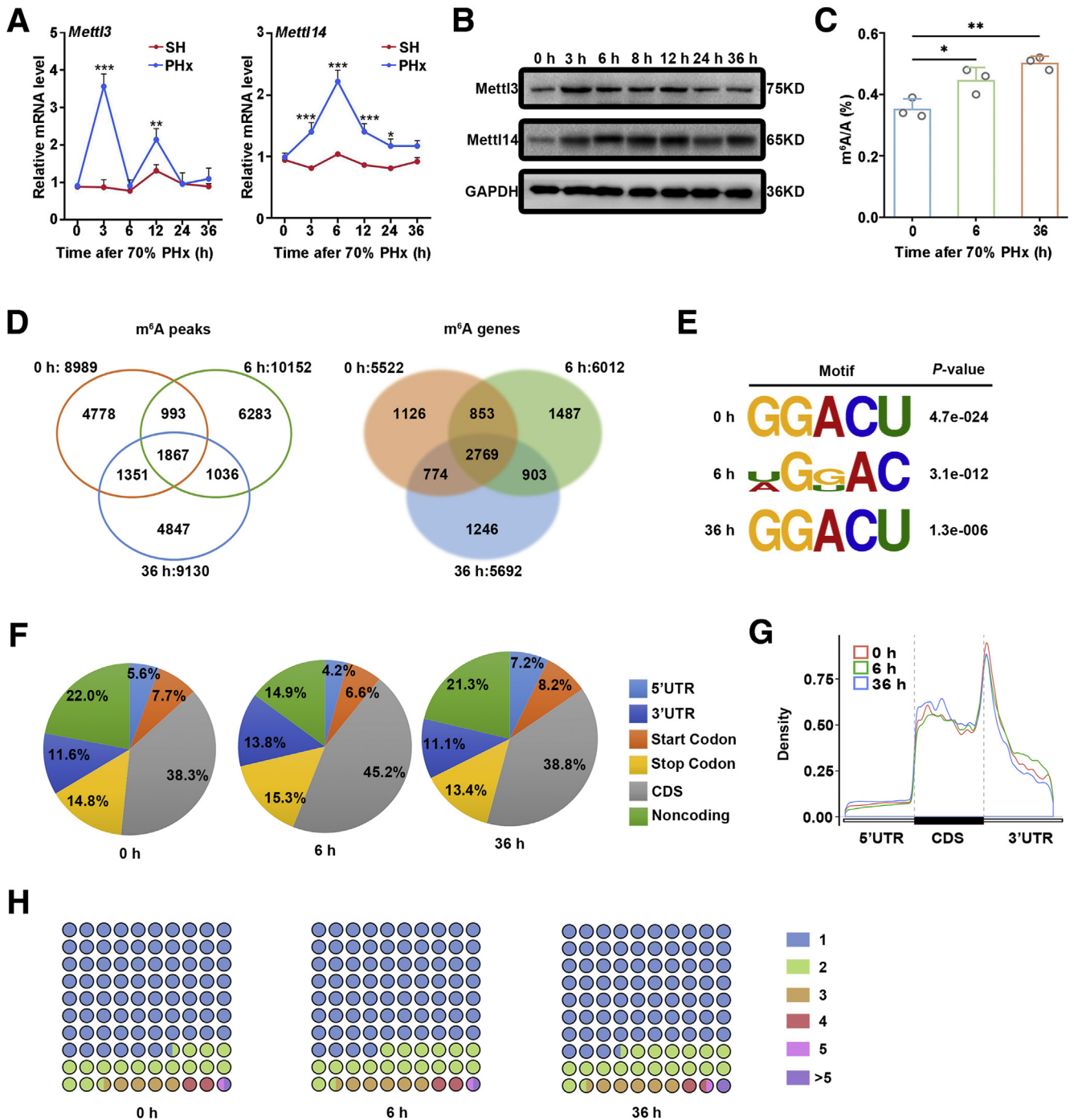


**Figure 1. Overview of m<sup>6</sup>A in the mouse liver after hepatectomy.** (A and B) qPCR and Western blotting show increased Mettl3 and Mettl14 levels at 6 hours after PHx.  $n = 3-5$ . (C) Total m<sup>6</sup>A level during liver regeneration detected by colorimetric.  $n = 3-5$ . (D) Venn diagram shows overlap of m<sup>6</sup>A peaks and m<sup>6</sup>A genes in 3 phases of liver regeneration. (E) Consensus motifs were identified by HOMER analysis with m<sup>6</sup>A peaks found in 3 phases of liver regeneration. (F) Metagenome distribution of m<sup>6</sup>A peaks in transcripts. (G) Proportion of total m<sup>6</sup>A peak distribution in the indicated regions. (H) Proportion of genes harboring different numbers of m<sup>6</sup>A peaks. Bar graphs: mean  $\pm$  standard deviation. \* $P < .05$ , \*\* $P < .01$ , \*\*\* $P < .001$ . SH, sham.

We next performed transcriptome-wide m<sup>6</sup>A mRNA sequencing (m<sup>6</sup>A-seq) to further characterize the m<sup>6</sup>A expression pattern during liver regeneration. In liver tissues collected from 3 representative phases of liver regeneration, basal state (quiescent liver or 0 hours after PHx), early phase (6 hours after PHx), and active phase of hepatocyte

mitosis (36 hours after PHx), we identified 8989, 10152, and 9130 m<sup>6</sup>A peaks, corresponding to 5522, 6012, and 5692 coding genes, respectively (Figure 1D). Among these genes, 2769 genes were found to be constantly methylated in all 3 phases, and 1126, 1487, and 1246 genes were uniquely methylated at 0, 6, and 36 hours after PHx,

respectively (Figure 1D). Consistent with a previous report,<sup>22</sup> the GGACU motif was highly enriched within m<sup>6</sup>A peaks (Figure 1E), and the m<sup>6</sup>A peaks were mostly enriched in the coding sequence (CDS) and around stop codons (Figure 1F and G). Among the potent m<sup>6</sup>A-modified genes, more than 70% of the genes had only 1 m<sup>6</sup>A site, and genes with 2 or more m<sup>6</sup>A sites accounted for 26.3% and 25.8% of the total m<sup>6</sup>A-modified genes at 6 and 36 hours after PHx, respectively, which were slightly higher than those in the quiescent liver (23.7%) (Figure 1H).

To understand the changes in m<sup>6</sup>A levels in genes, we compared the abundance (normalized to input) of m<sup>6</sup>A peaks between different phases. In total, compared with 0 hour, there were 2397 m<sup>6</sup>A peaks, corresponding to 1295 genes, which showed a significant increase in abundance in 6 hours after PHx, indicating that the proportion of m<sup>6</sup>A-modified mRNA transcripts was increased, and these m<sup>6</sup>A peaks were termed *hyperpeaks*; correspondingly, 988 m<sup>6</sup>A peaks (from 419 genes) showed a decrease and were termed *hypopeaks* (Figure 2A). Comparing the 6-hour and 36-hour time points, 788 m<sup>6</sup>A hyperpeaks (from 587 genes) and 2916 hypopeaks (from 620 genes) were identified (Figure 2B), indicating that many m<sup>6</sup>A-modified transcripts were demethylated with the progress of liver recovery. GO enrichment analysis showed that genes with hyperpeaks were clustered in the categories closely related to protein processing (such as protein modification and protein folding) and proliferation (such as the mitogen-activated protein kinase [MAPK] cascade, cell proliferation, extracellular signal-regulated kinase [ERK] cascade, cell cycle, and phosphatidylinositol 3-kinase [PI3K] signaling) (Figure 2C).

We then examined the dynamic m<sup>6</sup>A levels at 0, 6, and 36 hours after PHx. According to the different changes in the abundance of m<sup>6</sup>A peaks with time, these genes were artificially distributed into 4 quadrants (Figure 2D). An overwhelming proportion of m<sup>6</sup>A-modified genes (646/675) were increased in the early phase (6 hours vs 0 hours) and then decreased with the progression of regeneration (36 hours vs 6 hours), which corresponded to changes in the *Mettl3* and *Mettl14* levels in the same periods and suggested that m<sup>6</sup>A modification plays a critical role in regulating liver regeneration, particularly in the early phase. One gene from each quadrant was chosen for visualization analysis (Figure 2E). For example, visualization analysis of the *Rab20* gene illustrated that very few m<sup>6</sup>A peaks in *Rab20* transcripts were identified in the quiescent liver; however, the m<sup>6</sup>A peaks were notably increased at 6 hours and then decreased at 36 hours after PHx. GO enrichment analysis revealed that genes in the same quadrant as *Rab20* (lower-right quadrant) were primarily clustered in the categories of protein metabolism, protein modification, protein transport, cell proliferation, and stress response (Figure 2F).

### Liver-Specific *Mettl3* or *Mettl14* Deficiency Does not Impair Liver Homeostasis

To further elucidate the role of m<sup>6</sup>A in liver regeneration, we generated *Mettl3* or *Mettl14* liver-specific knockout mice (*Mettl3*-KO and *Mettl14*-KO mice, respectively) using the

albumin-Cre/loxp system as described previously (Figure 3A and B).<sup>16</sup> *Mettl3*-KO or *Mettl14*-KO did not affect the expression of m<sup>6</sup>A erasers, whereas WTAP was slightly increased (Figure 3C). Either *Mettl3* or *Mettl14* deficiency significantly decreased the global m<sup>6</sup>A levels in the liver (Figure 3D); however, all *Mettl3*-KO and *Mettl14*-KO mice were born and grew normally without any defect in the liver structure or glycolipid metabolism, and no spontaneous tumor was observed throughout their lifetimes (Figure 3E–G). It was likely that aberrant m<sup>6</sup>A modification caused by the loss of *Mettl3* or *Mettl14* did not disturb liver homeostasis under normal physiological conditions.

### *Mettl14* but not *Mettl3* Depletion Impairs Liver Regeneration After PHx

We next performed 70% PHx on KO and wild-type (WT) mice. In *Mettl3*-KO livers, the histologic structure and proliferation indexes were consistent with those of the WT livers (Figure 4), suggesting that loss of *Mettl3* did not have a noticeable effect on liver regeneration. In contrast, *Mettl14* ablation greatly delayed liver recovery, demonstrated as a much lower liver weight/body weight ratio and 5-bromo-2-deoxyuridine (BrdU) and Ki67 indexes at each time point (Figure 5A and B). Because Ki67 is initially expressed at the mid-G1 phase of the cell cycle,<sup>23</sup> the decreased Ki67 index together with the suppressed levels of G1-phase markers such as CyclinD1 and CDK4 suggest that *Mettl14* deficiency impaired liver regeneration and blocked hepatocytes in the G1 phase (Figure 5C). In addition, the expression of the S phase markers CyclinE1, CyclinA2, and CDK2 were significantly reduced in *Mettl14*-KO mice; the expression of CyclinB1, CDK1, and p-H3S10, which are the G2/M phase markers, were also decreased in *Mettl14*-KO liver (Figure 5C).

In addition to the slower recovery of the liver mass, serum assays indicated that the levels of alanine aminotransferase (ALT) and aspartate aminotransferase (AST) in *Mettl14*-KO mice were sustained at much higher levels after surgery than those in WT mice (Figure 5D and E). Histologically, the *Mettl14*-KO livers exhibited apparent necrosis as early as 6 hours after PHx, and the necrotic areas were further enlarged and could not be repaired even 72 hours after PHx (Figure 5F and G). The necrotic hepatocytes were characterized by a retained shape, lightly stained cytoplasm, and loss of nuclei. Hemorrhage and inflammatory infiltration were frequently observed (Figure 5F). In addition, cleaved caspase-3 immunohistochemistry staining showed notably increased apoptosis in the regenerating *Mettl14*-KO liver (Figure 5H and I). Together, *Mettl14* ablation in hepatocytes not only disrupted proliferation but also caused cell death, which was relatively rare. The results also highlighted the critical role of *Mettl14* in facilitating liver regeneration.

### Identifying Potential Targets of *Mettl14*

To further identify the role of *Mettl14*-mediated m<sup>6</sup>A modification in liver regeneration, we conducted m<sup>6</sup>A-seq in livers at 6 hours after PHx. The GGACU motif and m<sup>6</sup>A peak

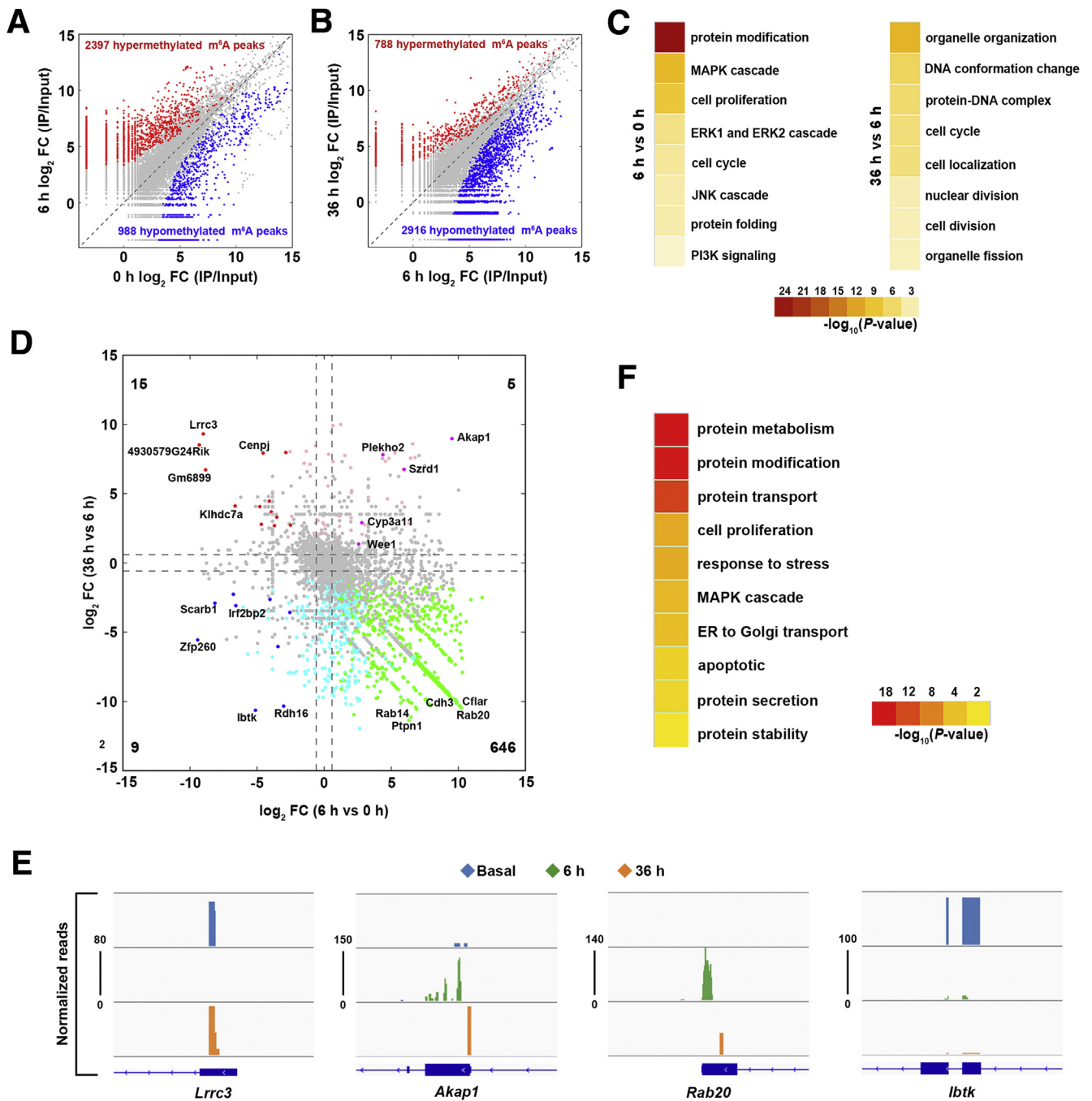


**Figure 2. The m<sup>6</sup>A level is dynamically changed during liver regeneration.** (A) Comparison of abundance of m<sup>6</sup>A peaks in 6 hours after PHx and quiescent livers. (B) Comparison of abundance of m<sup>6</sup>A peaks at 6 and 36 hours after PHx. (C) GO enrichment analysis indicates the biological process category of genes with significantly changed m<sup>6</sup>A level after hepatectomy. (D) Distribution of genes with dynamically changed m<sup>6</sup>A abundance during liver regeneration. (E) The m<sup>6</sup>A abundances on representative mRNA transcripts by m<sup>6</sup>A-seq. (F) GO enrichment analysis indicating the biological process categories of the 646 genes that increased at 6 hours after PHx and then decreased at 36 hours after PHx. JNK, c-Jun NH2 terminal kinase.

distributions in the KO mice were consistent with those in the WT mice (Figure 6A). In total, 5251 m<sup>6</sup>A peaks, corresponding to 3856 genes, were identified in the Mettl14-KO livers, both of which were greatly reduced compared with those in the WT livers (Figure 6B). In the Mettl14-KO liver, 8223 peaks disappeared, and 3320 new peaks appeared; 3383 genes lost m<sup>6</sup>A methylation, and 1227 genes were

m<sup>6</sup>A-methylated; 1931 peaks and 2629 genes were found commonly in WT and Mettl14-KO livers. In addition, the proportion of genes with only 1 m<sup>6</sup>A peak was slightly higher in Mettl14-KO livers than in the WT control, whereas fewer genes contained 2 or more m<sup>6</sup>A peaks (Figure 6C). We identified 3059 hypopeaks and 852 hyperpeaks that corresponded to 1736 and 351 genes in Mettl14-KO livers,

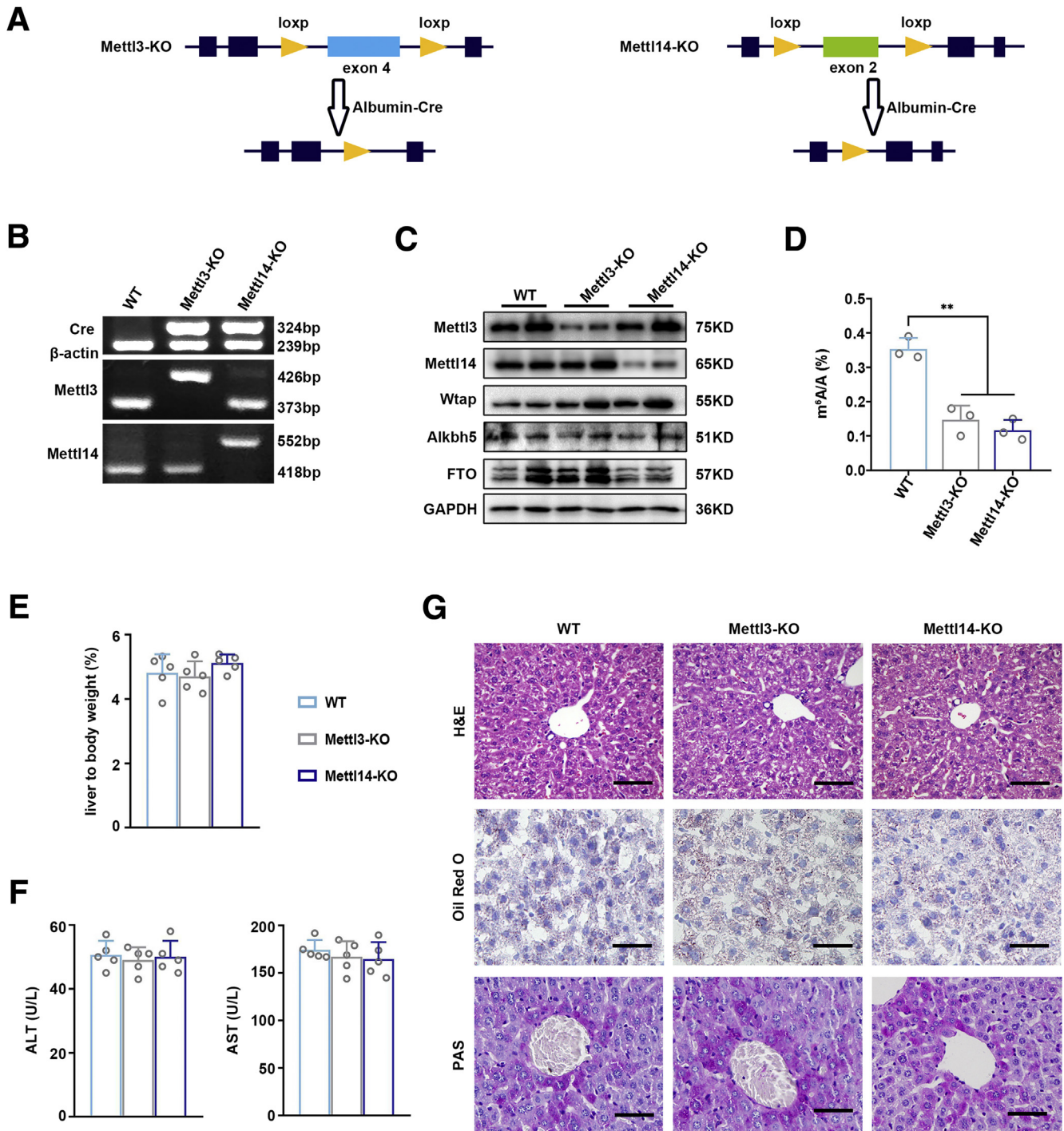


**Figure 3. Conditional Mettl3- and Mettl14-KO mice.** (A) Schematic diagram of strategy used to create liver-specific Mettl3- and Mettl14-KO mice. (B) Representative genotyping PCR results are shown. The  $\beta$ -actin gene was used as a positive control for the Cre gene. (C) Expression of  $m^6A$  writers and erasers in Mettl14-KO livers. (D) Total  $m^6A$  level in Mettl3- and Mettl14-KO mice detected by colorimetric analysis. (E and F) Ratio of liver weight/body weight and serum ALT and AST levels are normal in basic Mettl3-KO and Mettl14-KO mice. (G) H&E staining, oil red O staining, and PAS staining show regular hepatic lobule arrangement and normal glycolipid metabolism in the Mettl3-KO and Mettl14-KO quiescent livers (scale bar: 50  $\mu$ m). Bar graphs: mean  $\pm$  standard deviation;  $n = 3-5$ . \*\* $P < .01$ , \*\*\* $P < .001$ .

respectively, compared with those in WT controls (Figure 6D). Considering that Mettl14 is an  $m^6A$  writer, only the genes with reduced  $m^6A$  abundance ( $m^6A$  hypopeaks) in Mettl14-KO mice were considered potential Mettl14 targets,

and these genes were thereafter termed  $m^6A$  hypogenes. GO enrichment categories indicated that  $m^6A$  hypogenes were mainly clustered in protein modification and processing (Figure 6E). Remarkably, KEGG pathway analysis indicated

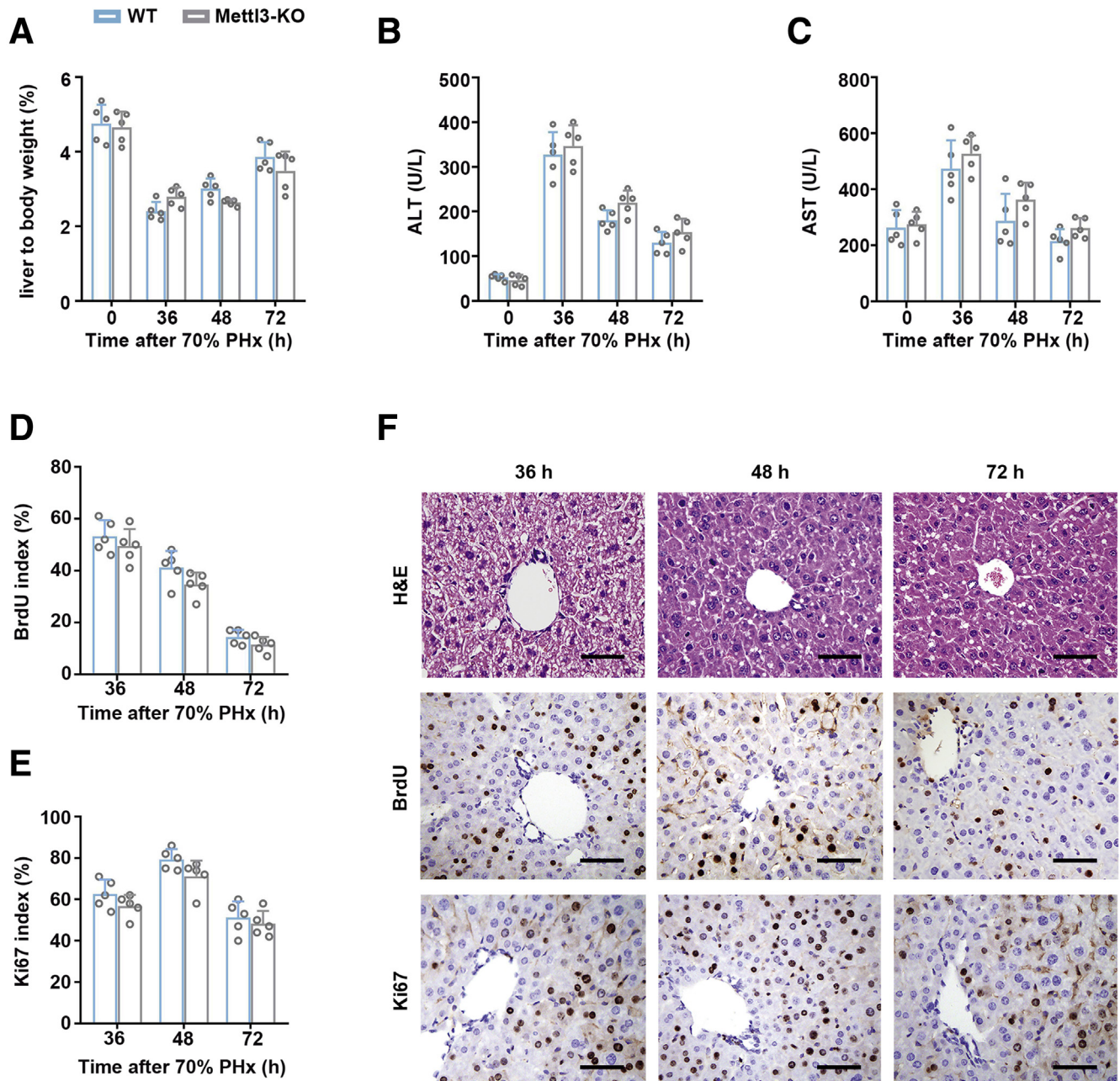


**Figure 4. Mettl3 deficiency is not sufficient to impair liver regeneration.** (A–C) Ratio of liver weight/body weight and serum ALT and AST levels are not significantly different in the regenerating Mettl3-KO and WT mice. (D and E) Calculation of BrdU- and Ki67-positive hepatocytes at indicated time points. (F) H&E staining shows histologically regenerating liver structures in Mettl3-KO mice. Immunohistochemistry for BrdU and Ki67 detection shows a similar proliferation capacity in the Mettl3-KO and WT livers (scale bar: 50 μm). Bar graphs: mean ± standard deviation; n = 3–5.

that these genes were significantly enriched in the transcripts encoding proteins responsible for polypeptide chain folding, modification, and transport in the ER (Figure 6F).

### *Mettl14 Deletion Induces Excessive ER Stress in the Regenerating Liver*

In the early stage of liver regeneration, a large number of polypeptide chains are necessary for generating new cell influx into the ER. Normally, hepatocytes activate the

unfolded protein response (UPR) and then enhance the expression of polypeptide-processing proteins, which are essential in ER homeostatic maintenance and are always activated during ER stress.<sup>24,25</sup> Because unresolved ER stress can lead to regeneration defects and even hepatocyte death,<sup>26,27</sup> together with hypogenes being mainly involved in protein modification and processing in the ER, we speculated that loss of Mettl14 might cause unresolved ER stress in regenerating hepatocytes. Transmission electron microscopy showed typical morphology of excessive ER stress in

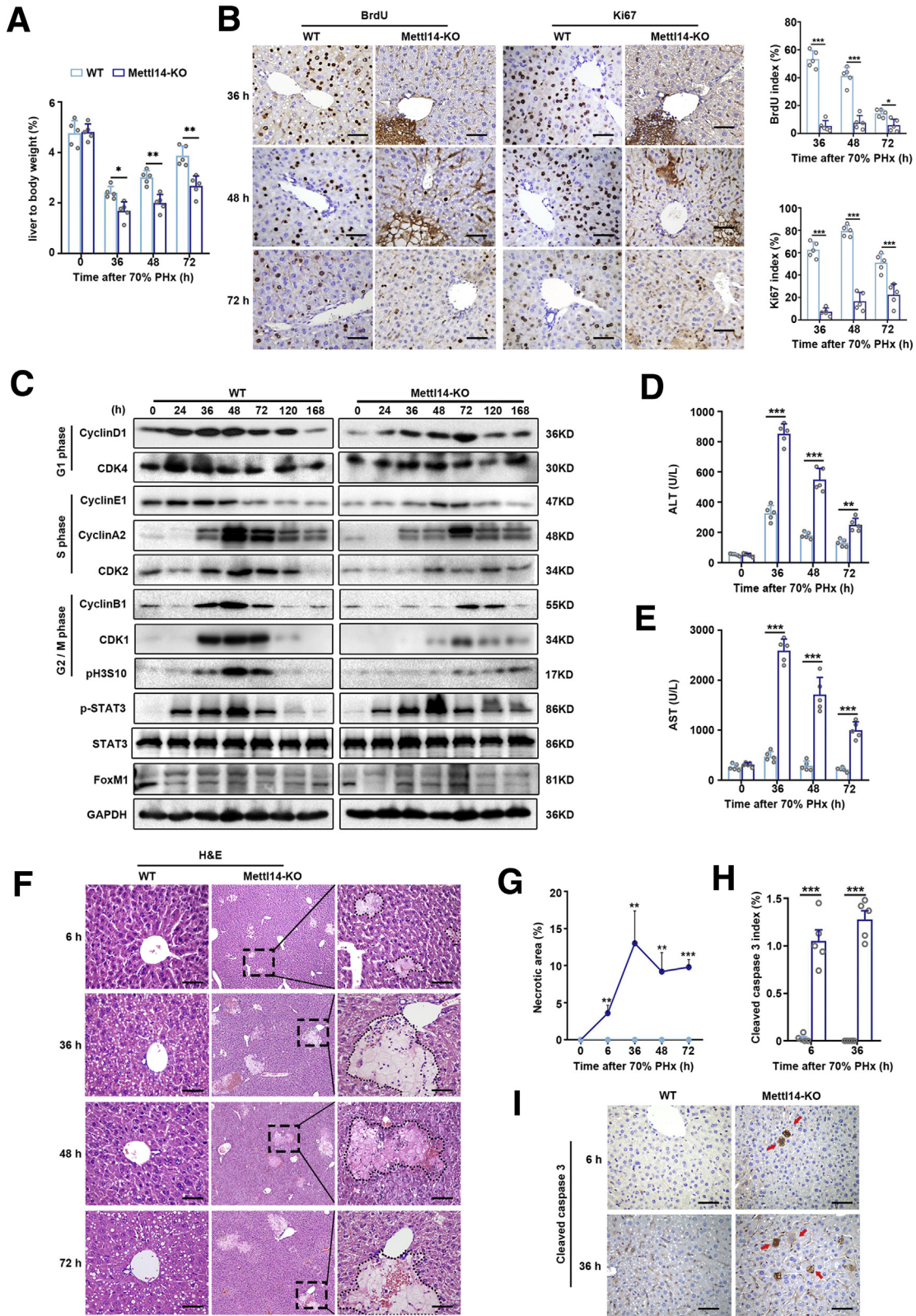


**Figure 5. Impaired liver regeneration in Mettl14-KO livers.** (A) Ratio of liver weight to body weight at indicated time points after PHx. (B) Immunohistochemistry results for BrdU and Ki67 indicate decreased proliferation rates in regenerating Mettl14-KO livers (scale bar: 50  $\mu$ m). (C) Western blotting analyses of cell cycle proteins. (D and E) Increased serum ALT and AST levels were increased in Mettl14-KO mice after PHx. (F) H&E staining shows parenchymal necrosis in the regenerating Mettl14-KO liver (scale bar: 50  $\mu$ m). Necrotic areas are circumscribed with dotted lines. (G) Percentage of necrotic areas. (H and I) Immunohistochemistry and quantitation of cleaved caspase-3 hepatocytes (scale bar: 50  $\mu$ m). Arrows indicate cleaved caspase-3-positive hepatocytes. Bar graphs: mean  $\pm$  standard deviation; n = 3–5. \* $P$  < .05, \*\* $P$  < .01, \*\*\* $P$  < .001.

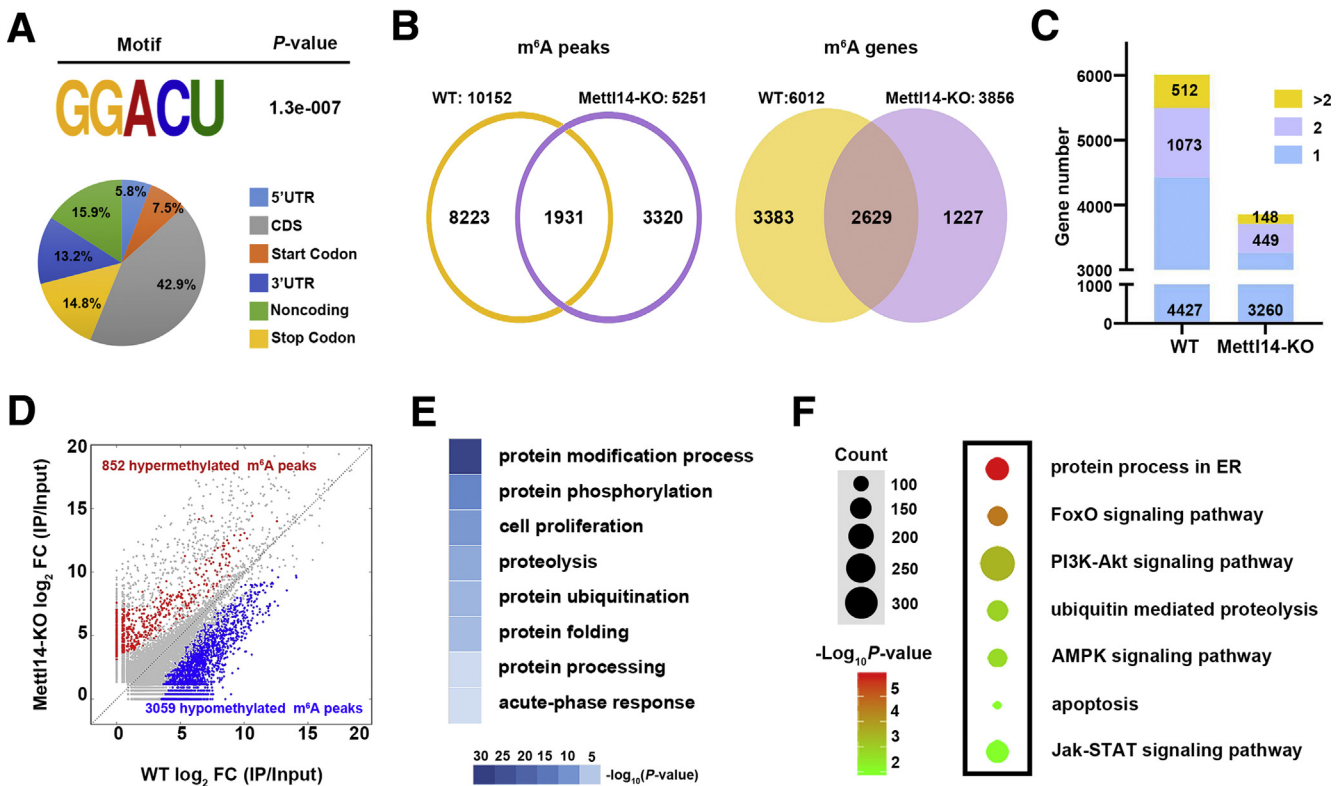


**Figure 6. Identification of potential Mettl14 targets by a transcriptome-wide m<sup>6</sup>A-seq assay.** (A) m<sup>6</sup>A motif and proportion of m<sup>6</sup>A peak distribution in the transcriptome of Mettl14-KO livers. (B) Number of m<sup>6</sup>A peaks and m<sup>6</sup>A-modified genes in WT and Mettl14-KO livers at 6 hours after PHx. (C) Proportion of genes harboring different numbers of m<sup>6</sup>A peaks. (D) Comparison of abundance of m<sup>6</sup>A peaks in Mettl14-KO and WT livers at 6 hours after PHx. (E) GO enrichment analysis indicating the biological process categories of genes with m<sup>6</sup>A hypopeaks. (F) Results from KEGG pathway analysis of the m<sup>6</sup>A hypogenes.

the Mettl14-KO liver, including extremely dilated or even fragmented ER, damaged mitochondria with fragmented cristae, and concentrated nuclei (Figure 7A). Moreover, examination of the UPR signaling cascades in Mettl14-KO livers revealed activation of ER stress sensors, such as p-inositol requiring enzyme 1 alpha (IRE1 $\alpha$ ), p-protein kinase R-like endoplasmic reticulum kinase (PERK), and activating transcription factor 6 (ATF6), as well as increased protein and/or mRNA levels of their downstream target genes such as X-box-binding protein 1 (XBP1), p-eukaryotic translation initiator factor 2 $\alpha$  (eIF2 $\alpha$ ), Bip, and the proapoptotic transcription factor C/EBP-homologous protein (Chop) (Figure 7B and C). Unresolved ER stress usually leads to cell death by up-regulating proapoptotic genes such as Chop and Bax and down-regulating the antiapoptotic gene Bcl2.<sup>28</sup> Increased Chop in ER stress further inactivates Akt/CyclinD1 and inhibits proliferation.<sup>29</sup> We observed decreased p-Akt, CyclinD1, and Bcl2 and increased Bax in regenerating Mettl14-KO livers (Figure 7B, Figure 5C).

To further confirm these findings, we transfected AML12 mouse liver cells with small interfering RNA targeting *Mettl14* in vitro. Mettl14 knockdown (Mettl14-KD) also resulted in increased Chop and Bax but decreased p-Akt, CyclinD1, and Bcl2 (Figure 8A). The Cell Counting Kit-8 assay and flow cytometry analysis showed suppressed cell growth and increased apoptosis in Mettl14-KD cells (Figure 8B and D–G).

AML12 cells were further treated with tunicamycin (TM) to stimulate ER stress as described previously.<sup>26</sup> TM treatment enhanced p-PERK, Chop, Bip, and Bax expression and decreased p-Akt, CyclinD1, and Bcl2 expression in AML12 cells (Figure 8A), resulting in more apoptosis and impaired cell growth (Figure 8C–G). Mettl14-KD in cells significantly aggravated the effect of TM on AML12 cells (Figure 8). Together, consistent with the in vivo findings, the absence of Mettl14 sensitized hepatocytes to excessive ER stress, resulting in cell cycle arrest and increased apoptosis and cell death.

### Transcripts of Polypeptide-Processing Proteins Are Regulated by Mettl14 in the Regenerating Liver

To further identify the Mettl14-target genes involved in ER homeostasis, we reviewed the m<sup>6</sup>A-seq results and performed the m<sup>6</sup>A-RIP-qPCR assay. The m<sup>6</sup>A abundance on transcripts encoding polypeptide-processing proteins in the ER was significantly decreased in the Mettl14-ablated livers (Figure 9A). *Hsp90b1* and *Erp29* are responsible for polypeptide chain folding.<sup>30,31</sup> *Stt3a* is an N-oligosaccharyl-transferase and glycosylate polypeptide as it enters the lumen of the ER,<sup>32</sup> *P4hb* serves as the protein disulfide isomerase and ensures the correct arrangement of disulfide bonds in the ER,<sup>33</sup> and *Lman1* is a cargo receptor that

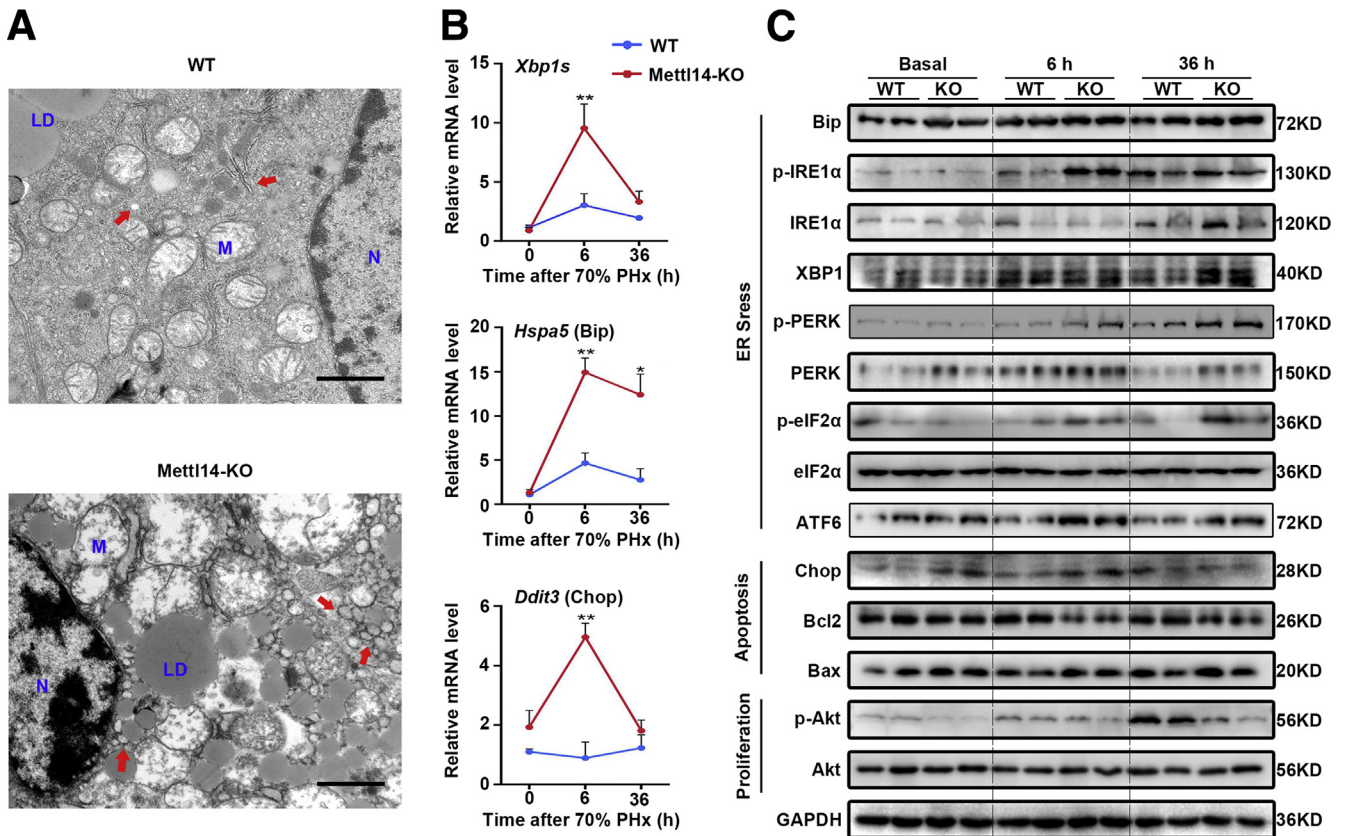


**Figure 7. Mettl14 deficiency leads to excessive ER stress after PHx.** (A) Representative images from transmission electron microscope analyses of hepatocytes from WT and Mettl14-KO mice. ER structure is highlighted by arrows. (scale bar: 1  $\mu$ m). (B and C) Western blotting and qPCR show activated ER stress markers and proapoptosis proteins and suppressed indexes of proliferation and antiapoptosis proteins in WT and Mettl14-KO mice. Bar graphs: mean  $\pm$  standard deviation; n = 3–5. \* $P$  < .05, \*\* $P$  < .01. LD, lipid droplets; M, mitochondria; N, nuclei.

circulates between the ER and Golgi compartment to transport proteins.<sup>34</sup> The m<sup>6</sup>A-RIP-qPCR assay showed a reduction in the m<sup>6</sup>A abundance on these mRNA transcripts in the Mettl14-KO livers (Figure 9B), and these transcripts were further determined to be directly bound by Mettl14 (Figure 9C). Thus, the mRNA and protein levels of the genes above were dramatically decreased in the Mettl14-KO liver at 6 hours after PHx (Figure 9D and E). Similarly, in TM-treated AML12 cells, all these proteins were markedly reduced in response to Mettl14-KD (Figure 8H).

To test whether the reduction in these polypeptide-processing proteins was due to impaired mRNA stability or translation, we isolated primary hepatocytes from WT and Mettl14-KO mice and treated the cells with actinomycin (Act D) for the mRNA stability assay as described previously.<sup>19,35</sup> All the included mRNA transcripts exhibited decreased stability in Mettl14-KO hepatocytes (Figure 9F). Moreover, RIP-qPCR revealed less binding of eukaryotic translation initiation factor 3 subunit A (EIF3A) to these transcripts in Mettl14-KO livers (Figure 9G), indicating a translation defect in these genes.

Among these included polypeptide-processing proteins, Hsp90b1 ablation was reported to evoke polypeptide accumulation, attenuate proliferation, and enhance apoptosis.<sup>30,36</sup> Similar to Mettl14-KD, Hsp90b1-KD in

AML12 cells elevated the expression of Bip, Chop, and Bax but decreased that of Bcl2, p-Akt, and CyclinD1 (Figure 10A), resulting in increased cell apoptosis, retarded cell growth, and arrested cell cycle (Figure 10B–F). These data suggest that the role of Mettl14 in liver regeneration is partly dependent on regulating the m<sup>6</sup>A modification of Hsp90b1.

### Inhibition of ER Stress Reduces Necrosis in Mettl14-Deficient Livers

To further verify that unresolved ER stress in Mettl14-KO mice was responsible for impaired liver regeneration, we treated mice with tauroursodeoxycholate (TUDCA), a chemical chaperone that reduces ER stress, 1 hour before PHx, as reported previously.<sup>37</sup> Although TUDCA treatment did not completely restore the impaired liver regeneration in Mettl14-KO mice, the necrotic area and inflammatory infiltration were significantly decreased (Figure 11A and B). The BrdU and Ki67 indexes in Mettl14-KO mice treated with TUDCA were partially restored (Figure 11A, C, and D). In addition, the expression of p-IRE1 $\alpha$ , Chop, and Bax was reduced and the expression of p-Akt, CyclinD1, and Bcl2 was slightly increased in Mettl14-KO mice with TUDCA treatment after PHx (Figure 11E). Taken together, our results

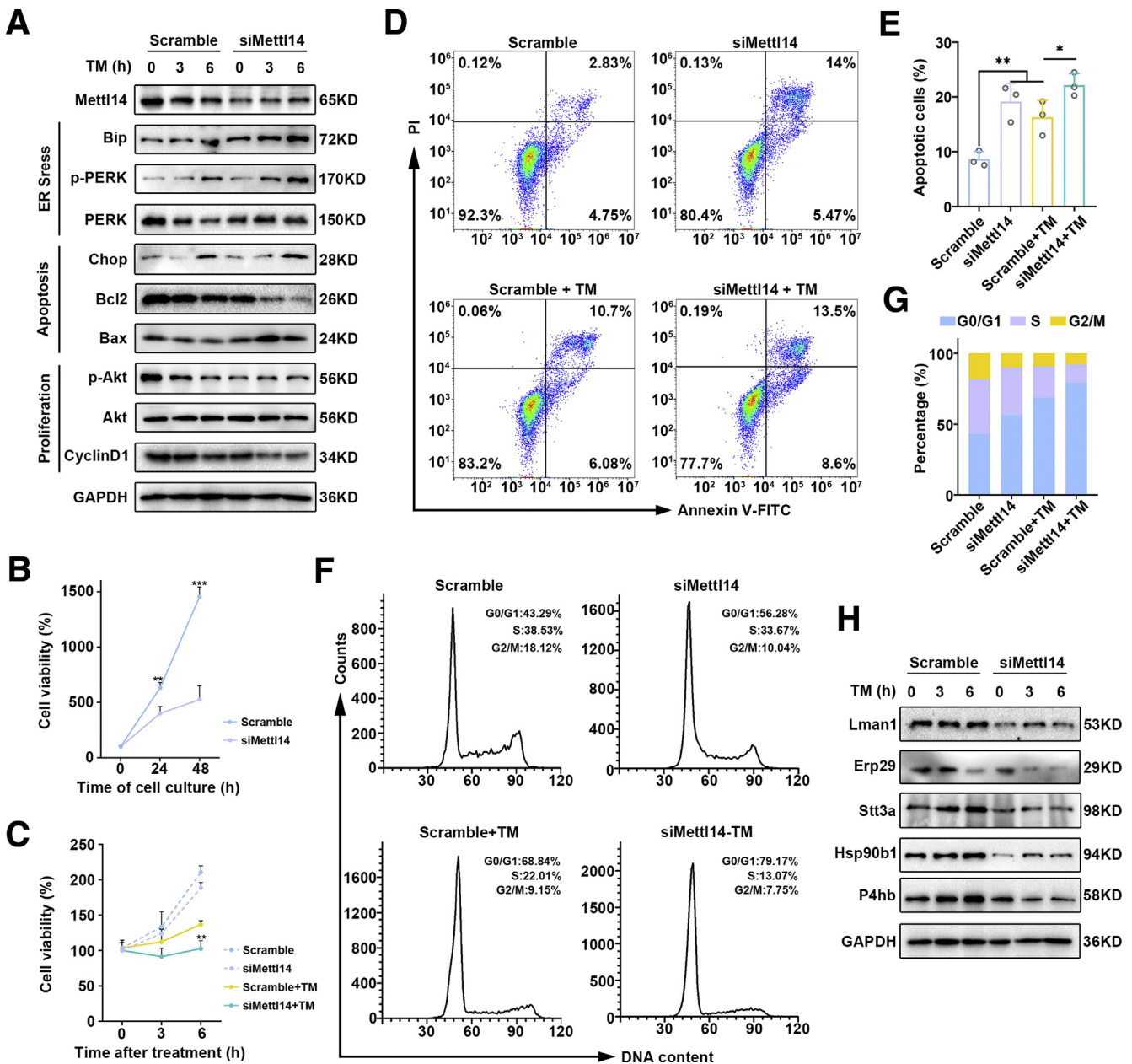


**Figure 8. Mettl14-KD induces excessive ER stress in vitro.** (A) AML12 cells were transduced with siMettl14 and treated with TM at final concentration of 5  $\mu$ g/mL. Western blotting shows activated ER stress markers and proapoptosis proteins and inactivated the indexes of proliferation in Mettl14-KD cells. (B) Viability of AML12 was tested at indicated time points after Mettl14-KD using a CCK-8 kit. (C) Cell viability was tested after TM treatment using a CCK8 kit. (D and E) Flow cytometry analysis shows increased apoptosis rate in Mettl14-KD cells after TM treatment. (F and G) Flow cytometry analysis of cell cycle distributions of AML12 cells treated with TM. (H) Western blotting shows decreased expression of the indicated genes in Mettl14-KD AML12 cells after TM treatment. Bar graphs: mean  $\pm$  standard deviation; n = 3–5. \* $P$  < .05, \*\* $P$  < .01, \*\*\* $P$  < .001. siMettl, small interfering methyltransferase-like.

further demonstrate that ER stress, regulated by Mettl14, plays a crucial role in facilitating liver regeneration, and TUDCA treatment partially prevents ER stress and ameliorates hepatocyte necrosis in Mettl14-KO mice.

## Discussion

Epigenetic modifications are required for liver regeneration.<sup>23,38–40</sup> However, the role of m<sup>6</sup>A modification in liver

regeneration remains obscure. In this study, we revealed dynamic changes in m<sup>6</sup>A modifications during liver regeneration and demonstrated that Mettl14-mediated m<sup>6</sup>A plays a critical role in liver regeneration by regulating the expression of polypeptide-processing proteins and maintaining ER homeostasis.

Similar to most epigenetic modifications, m<sup>6</sup>A is dynamic and reversible.<sup>6</sup> The methyltransferase complex, containing

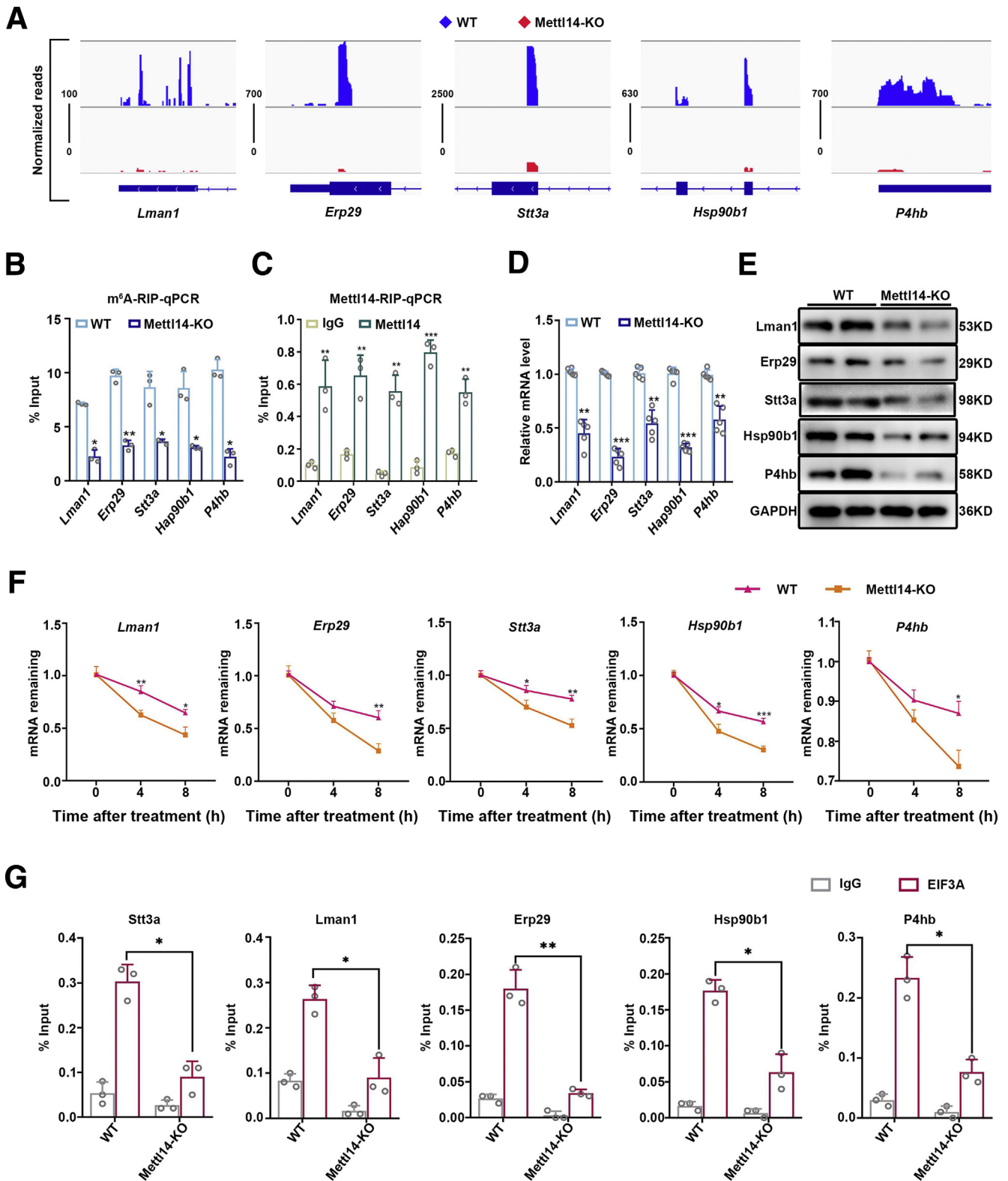


**Figure 9. Mettl14 regulates stability and translation of polypeptide chain-processing protein transcripts.** (A) The  $m^6A$  abundance of indicated mRNA transcripts in the WT and Mettl14-KO livers as determined by  $m^6A$ -seq. (B) The  $m^6A$ -RIP-qPCR assay shows reduced  $m^6A$  modification on indicated mRNA transcripts in Mettl14-KO livers. (C) RIP-qPCR shows association of indicated mRNA transcripts with Mettl14 in WT livers. (D and E) qPCR and Western blotting show decreased expression of indicated genes in Mettl14-KO livers. (F) qPCR of indicated transcripts in ActD-treated primary hepatocytes shows decreased mRNA stability in Mettl14-KO hepatocytes. (G) RIP-qPCR shows decreased association of EIF3A with indicated transcripts in Mettl14-KO livers. Bar graphs: mean  $\pm$  standard deviation;  $n = 3-5$ . \* $P < .05$ , \*\* $P < .01$ , \*\*\* $P < .001$ .

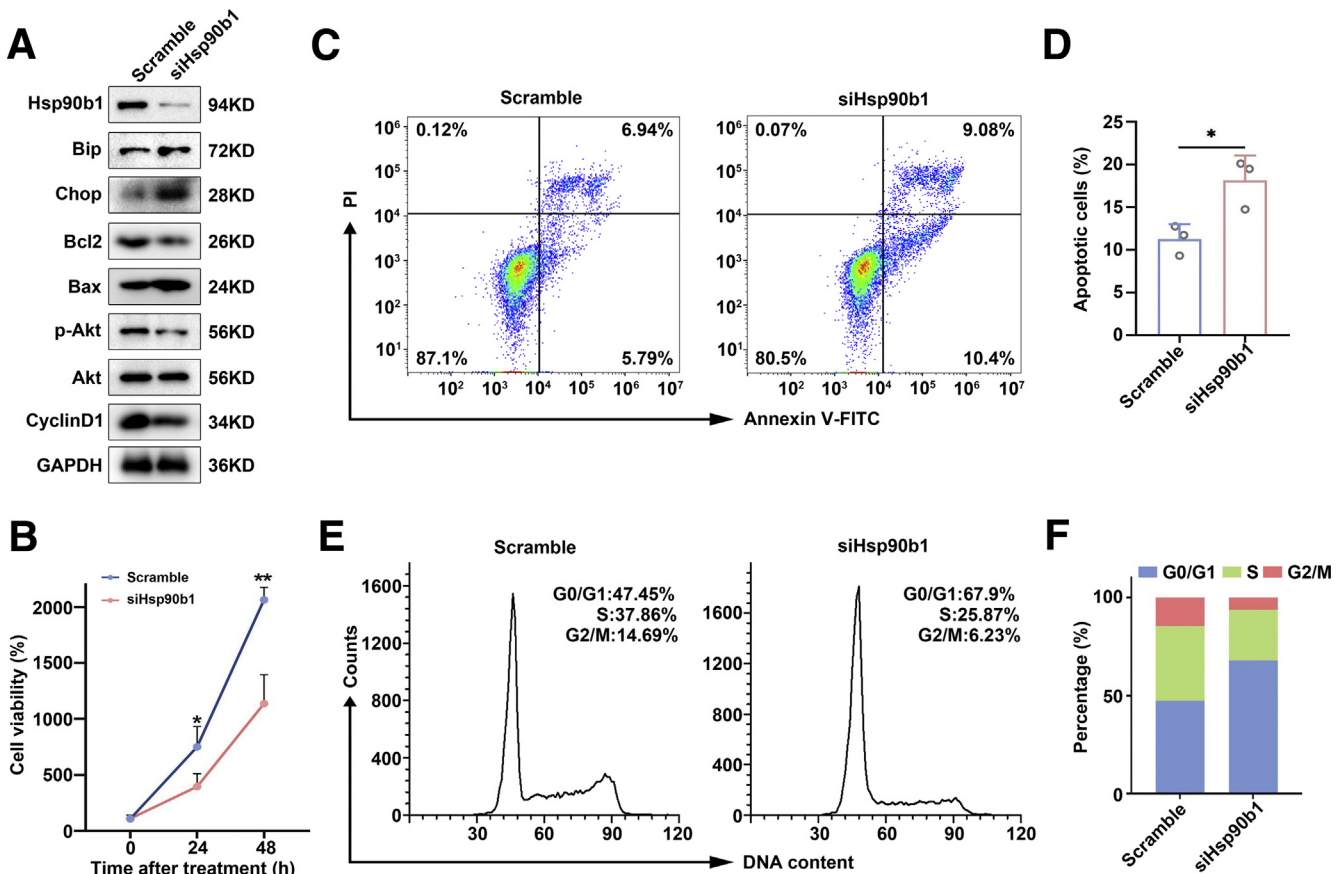


**Figure 10. Hsp90b1 is a critical target of Mettl14 that inhibits proliferation and promotes apoptosis.** (A) AML12 cells were transduced with siHsp90b1. Western blotting shows changes in levels of proteins involved in ER stress, apoptosis, and proliferation. (B) CCK-8 assays show suppressed cell growth after Hsp90b1-KD. (C and D) Flow cytometry analysis shows increased apoptosis rate in Hsp90b1-KD cells. (E and F) Flow cytometry assays show that the cell cycle is arrested in the G0/G1 phase after Hsp90b1-KD. Bar graphs: mean  $\pm$  standard deviation;  $n = 3-5$ . \*\* $P < .01$ , \*\*\* $P < .001$ .

Mettl3, Mettl14 and WTAP, is responsible for installing  $m^6A$  on mRNA.<sup>6</sup> Systemic ablation of any member of the  $m^6A$  methyltransferase complex leads to embryonic death,<sup>41,42</sup> highlighting the critical role of  $m^6A$  in diverse physiological processes. Similar to the dynamic changes in Mettl3 and Mettl14 expression after PHx, most of the  $m^6A$ -modified genes underwent initial up-regulation and subsequent down-regulation of  $m^6A$  modulation after PHx. This trend was coincident with the dramatic activation and modification of numerous genes involved in the same stage. Our data strongly support that  $m^6A$  modification is a key molecular event in regulating liver regeneration.

The loss of Mettl14 impaired liver regeneration to a dramatically greater extent than Mettl3 ablation. We also generated liver-specific WTAP-deficient mice, and surprisingly, most of these mice died within 25 days of birth (data not shown). These findings suggest the different roles of each  $m^6A$  writer in the same biological process. Mettl3 is the catalytic unit, and Mettl14 is the allosteric adaptor, which enhances the catalytic activity of Mettl3 and helps Mettl3 recognize the substrate RNA. Mettl3 and Mettl14 can play similar roles because the loss of either Mettl3 or Mettl14 results in spermatogonial stem cell depletion.<sup>16</sup> However,

previous in vitro studies showed that Mettl3 and Mettl14 have opposite roles in regulating liver cancer cell and leukemia cell proliferation by targeting different genes.<sup>19-21,43</sup> It would be interesting to determine why the loss of Mettl3 does not significantly disturb liver homeostasis or regeneration. Huang et al<sup>44</sup> found that histone H3 trimethylation H3K36me3 binds to Mettl14 and recruits methyltransferase complex to deposit  $m^6A$  on newly synthesized mRNA. With in-depth studies on methyltransferase, an increasing number of factors have been identified as members of the complex. Therefore, different signaling pathways in different cells may combine with different members of the complex to specifically regulate the genes related to a biological process. The separate role of each subunit in the Mettl3-Mettl14-WTAP complex is far from clear and requires further characterization.

Interestingly, Mettl14 deficiency does not affect liver homeostasis but dramatically impairs liver regeneration after PHx. In response to regeneration stimuli, a large number of genes, including Mettl14, are rapidly activated in the remaining hepatocytes, suggesting that Mettl14 is also triggered by mitotic signals. CEBP $\alpha$  and CEBP $\beta$ , which were identified as necessary to promote liver

regeneration,<sup>45,46</sup> are potential transcription factors that bind to the *Mettl14* gene.<sup>19</sup> Therefore, the role of *Mettl14*-mediated m<sup>6</sup>A seems to depend on the activation of mitotic signals and provides a reasonable explanation for why *Mettl14* ablation does not obviously disturb homeostasis in quiescent livers.

One of the most interesting findings in our study is that the hepatic loss of *Mettl14* resulted in necrosis in regenerating livers, an event that is very rarely observed in the surgical model of liver regeneration. This finding led to our speculation that impaired liver regeneration is not solely attributed to cell cycle arrest. In the regenerating liver, a large amount of newly synthesized peptides enter the ER, where they are further processed into functional proteins to produce new hepatocytes. In this context, the defect in UPR can be caused by the deficiency in ER stress sensors, such as IRE1 $\alpha$  and XBP1, or the insufficient production of polypeptide-processing proteins, such as Hsp90b1, leading to unresolved ER stress.<sup>26,27,30</sup> Unresolved ER stress further leads to impaired cell growth and even cell death, as observed in IRE1 $\alpha$ -, XBP1-, or Hsp90b1-deficient livers.<sup>26,27,30</sup> The similar histologic changes in the *Mettl14*-ablated regenerating liver strongly suggests the development of unresolved ER stress in the mutant liver. Examination of ER morphology and ER stress markers confirmed the excessive ER stress in *Mettl14*-KO regenerating livers. Treatment with TUDCA effectively reduced ER stress and partly rescued the impaired liver regeneration, especially the necrosis in *Mettl14*-ablated livers, providing further evidence of the association between *Mettl14* inactivation and ER homeostasis.

m<sup>6</sup>A affects the stability and translation of mRNA transcripts. We identified a group of m<sup>6</sup>A hypogenes that encode polypeptide-processing proteins in the ER, and their stability and translation were impaired, resulting in decreased RNA and protein levels in the *Mettl14*-KO livers. We did not observe that genes encoding ER stress sensors are m<sup>6</sup>A targets, indicating that their increase in the *Mettl14* KO liver is an adaptive response to the defect in polypeptide processing but not directly regulated by *Mettl14*.

*Mettl14* deletion also resulted in hepatocyte cycle arrested in G1 phase. On the one hand, ER stress in *Mettl14*-KO liver led to increased Chop, thus inhibiting p-Akt-Cyclin D1 pathway.<sup>47</sup> On the other hand, m<sup>6</sup>A hypogenes in *Mettl14*-KO mice were also enriched in PI3K-Akt pathway, which is important in hepatocyte proliferation during liver regeneration. Therefore, *Mettl14* deletion may also block cell cycle by inhibiting PI3K-Akt pathway, which needs further proof. It should be noted that the polypeptide-processing proteins constitute only one portion of the *Mettl14* target genes. Therefore, we cannot exclude the possibility that other genes with altered m<sup>6</sup>A levels are induced by *Mettl14* deficiency and impair liver regeneration. In addition, the m<sup>6</sup>A abundance was increased in some transcripts in the *Mettl14*-KO regenerating liver, and the deficiency of any methyltransferase alone or in combination did not cause the complete disappearance of the m<sup>6</sup>A modifications,<sup>16</sup> suggesting that m<sup>6</sup>A is comprehensively regulated and many other writers may be involved.

In summary, we have provided in vivo evidence that the m<sup>6</sup>A methyltransferase *Mettl14*, but not *Mettl3*, plays an essential role in promoting liver regeneration at least partly through the deposition of m<sup>6</sup>A on the mRNA transcripts of polypeptide-processing proteins in the ER, thereby maintaining ER homeostasis (Figure 11F).

## Methods

### Mice and Treatments

The experiments were approved by the Animal Care and Use Committee of Sichuan University. *Mettl3*<sup>loxP/loxP</sup> and *Mettl14*<sup>loxP/loxP</sup> were provided by Dr M. H. Tong, Shanghai Institute of Biochemistry and Cell Biology, University of Chinese Academy of Sciences. Albumin-Cre transgenic mice were purchased from Shanghai Biomodel Organism Science, and the genotypes of the Albumin-Cre, *Mettl3*<sup>loxP/loxP</sup> and Albumin-Cre, *Mettl14*<sup>loxP/loxP</sup> mice were determined using PCR amplification of tail DNA. PHx was performed on 8-week-old male mice as described previously.<sup>23</sup> BrdU (1 mg/kg body weight; cat. B5002, Sigma-Aldrich, St Louis, MO) was intraperitoneally injected 60 minutes before the mice were killed. TUDCA (75  $\mu$ g/g body weight; cat. T0266, Sigma-Aldrich) was intravenously injected 1 hour before PHx.

### m<sup>6</sup>A Sequencing

CloudSeq Biotech Inc (Shanghai, China) performed m<sup>6</sup>A-seq. Total RNA was extracted from mouse liver tissue and then randomly fragmented. A specific anti-m<sup>6</sup>A antibody (cat. 202003; Synaptic Systems, Goettingen, Germany) was applied for the m<sup>6</sup>A pull-down assays. A TruSeq Stranded mRNA Sample pre-kit (Illumina, San Diego, CA) was used to construct a library from both input and m<sup>6</sup>A IP samples, which were then deeply sequenced on an Illumina HiSeq instrument in 2  $\times$  100 cycles of Solexa paired-end sequencing. The m<sup>6</sup>A-seq data were deposited in the Genome Sequence Archive (<https://bigd.big.ac.cn/gsa/>) under accession number CRA003378.

### Quantification of mRNA m<sup>6</sup>A

The m<sup>6</sup>A level in total RNA was assessed using an m<sup>6</sup>A RNA methylation quantification kit (cat. ab185912; Abcam, Cambridge, UK) according to the manufacturer's protocol. Briefly, 200 ng of total RNA was added to each well, and then the capture antibody solution and detection antibody solution were added. The absorbance at 450 nm was colorimetrically measured for m<sup>6</sup>A level.

### mRNA Isolation and Real-Time PCR

Total mRNA was purified from 25 mg of liver tissue using an RNA Isolation kit (cat. RE-03011; Foregene, Chengdu, China). mRNA was reverse transcribed to cDNA using the iScriptcDNA Synthesis kit (cat. 179-8890; Bio-Rad, Hercules, CA). A CFX Connect Real-Time System (Bio-Rad) was used for real-time PCR. The gene expression levels were normalized to GAPDH gene expression.

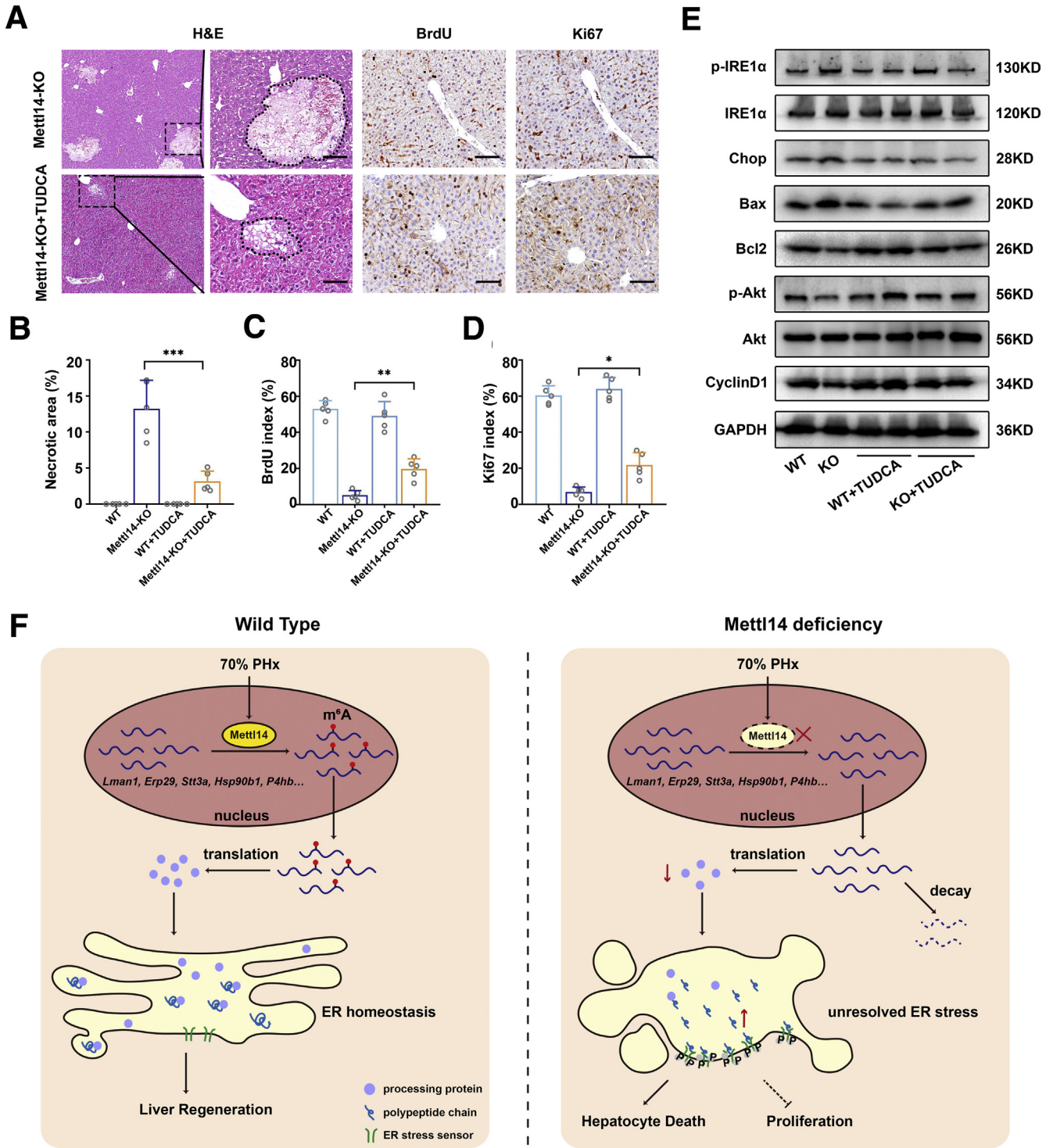


**Figure 11. TUDCA treatment partially restores liver regeneration in Mettl14-KO mice.** (A) H&E staining and BrdU and Ki67 immunohistochemistry results show partially restored liver regeneration in Mettl14-KO mice (scale bar: 50 μm). Necrotic areas are circumscribed with dotted lines. (B) Percentage of necrotic areas. (C and D) BrdU and Ki67 indexes show increased proliferation rates of Mettl14-KO mice with TUDCA treatment. (E) Western blotting shows decreased ER stress markers and proapoptosis proteins and increased indexes of proliferation and antiapoptosis proteins in Mettl14-KO mice treated with TUDCA. (F) Hypothetical model of Mettl14 during liver regeneration. Bar graphs: mean ± standard deviation; n = 3–5. \*P < .05, \*\*P < .01.

### Western Blotting

Liver tissues were homogenized for protein extraction. Sodium dodecyl sulfate-polyacrylamide gel electrophoresis and immunoblotting were performed, and an electrochemiluminescent reagent was used for chemiluminescence detection. Primary antibodies were Mettl3 (cat. A8370; Abclonal, Woburn, MA), Mettl14 (cat. HPA038002; Sigma-Aldrich), FTO (cat. ET1705-89; HUABIO, Woburn, MA), Alkbh5 (cat. ER65894; HuaBio), WTAP (cat. 56501; Cell Signaling Technology, Danvers, MA), Lman1 (cat. ab125006; Abcam), Erp29 (cat. ET7108-03; HuaBio), Stt3a (cat. 12034-1-AP; Proteintech, Rosemont, IL), Hsp90b1 (cat. ER1511-5; HuaBio), P4hb (cat. ER40404; HuaBio), Bip (cat. ER40402; HuaBio), p-IRE1 $\alpha$  (cat. NB100-2323; Novus Biologicals, Littleton, CO), IRE1 $\alpha$  (cat. 3294; Cell Signaling Technology), XBP1 (cat. Ab37152; Abcam), p-PERK (cat. 3179 Cell Signaling Technology), PERK (cat. 3192; Cell Signaling Technology), p-eIF2 $\alpha$  (cat. ET1603-14; HuaBio), eIF2 $\alpha$  (cat. RT1196; HuaBio), Chop (cat. ET1703-05; HuaBio), ATF6 (cat. EM1701-94; HuaBio), Cyclin D1 (cat. ab134175; Abcam), CDK4 (cat. ab199728; Abcam), Cyclin E1 (cat. ET1612-16; HuaBio), Cyclin A2 (cat. ET1612-26; HuaBio), Cyclin B1 (cat. 4138; Cell Signaling Technology), CDK1 (cat. ab32384; Abcam), p-STAT3 (cat. 9145; Cell Signaling Technology), STAT3 (cat. 9139; Cell Signaling Technology), forkhead box M1 (FoxM1) (cat. ER1706-62; HuaBio), p-Akt (cat. ET1607-73; HuaBio), Akt (cat. ET1612-16; ET1609-47), Bcl2 (cat. ET1702-53; ET1609-47), Bax (cat. 2772; Cell Signaling Technology), and GAPDH (cat. KC-5G4; KangChen Biotech, Shanghai, China).

### Immunohistochemistry

Liver specimens were fixed in 10% neutral buffered formalin for 36–48 hours. Paraffin sections (4  $\mu$ m thick) were prepared and performed a series of dewaxing, rehydration, antigen retrieval, and quenching of endogenous peroxidase activity. The sections were incubated with the corresponding primary antibody at 4°C overnight and anti-mouse/rabbit secondary antibody (Dako REAL EnVision Detection System, Glostrup, Denmark) for 1 hour at room temperature. Detection was developed using the 3,3'-diaminobenzidine substrate. Primary antibodies were cleaved caspase 3 (cat. 9664; Cell Signaling Technology), pH3S10 (cat. 06-570; Merck Millipore, Burlington, MA), BrdU (cat. MS-1058-P0; Thermo Fisher Scientific, Waltham, MA), and Ki67 (cat. RM-9106-S1; Thermo Fisher Scientific).

### Gene-Specific m<sup>6</sup>A qPCR

m<sup>6</sup>A-IP enrichment followed by real-time qPCR to quantify the changes in m<sup>6</sup>A methylation of the target gene was performed using the Magna MeRIP m<sup>6</sup>A Kit (cat. 17-10499; Millipore) following the manufacturer's instructions. Briefly, 5  $\mu$ g of fragmented mRNA was incubated with m<sup>6</sup>A antibody (cat. 202003; Synaptic Systems) or for 4 hours at 4°C. Methylated RNA was eluted and purified, and real-time qPCR was performed to analyze the relevant enrichment of m<sup>6</sup>A of target gene in each sample.

### RIP–Real-Time-qPCR Reaction

Liver tissues were homogenized in polysome lysis buffer, and 10% of the supernatant was collected as input. The Mettl14 antibody, EIF3A antibody (cat. 3411; Cell Signaling Technology), or immunoglobulin G-conjugated Protein A/G magnetic beads were added to the remaining supernatant and incubated at 4°C overnight. After washing, the immunoprecipitated RNAs and input were treated with Proteinase K at 55°C for 2 hours. RNA was recovered by phenol: chloroform extraction, followed by ethanol precipitation. Then real-time qPCR analyses were performed.

### Primary Hepatocyte Isolation

Primary hepatocytes were isolated using the collagenase perfusion method. The liver was perfused with prewarmed Hank's balanced solution and followed by digestion medium. Primary hepatocytes were counted and seeded on type I collagen-coated 6-well plates in low-glucose medium containing 10% fetal bovine serum, 2 mmol/L L-glutamine, and 100 U/mL of penicillin/streptomycin.

### mRNA Stability

Hepatocytes were treated with Act D (cat. A9415; Sigma-Aldrich) at a final concentration of 5  $\mu$ g/mL for 4 or 8 hours. Total RNA was purified by RNA Isolation kit and analyzed by real-time qPCR. The half-life of indicated mRNA was calculated as reported previously.<sup>19</sup> GAPDH was used for normalization.

### Transmission Electron Microscopy

Livers were prepared for electron microscopy by fixing the liver tissue with 2.5% glutaraldehyde in 0.1 mol/L phosphate salt buffer (pH 7.4) and then post-fixed in 0.1 mol/L cacodylate buffer (pH 7.2) with 1% osmium tetroxide. After dehydration, embedding, and sectioning, they were examined with JEM-1400PLUS microscope.

### Cell Culture and Small Interfering RNA Transfection

The AML12 mouse liver cell line was maintained in a 1:1 mixture of Dulbecco modified Eagle medium and Ham's F12 medium supplemented with 10% fetal bovine serum, 5  $\mu$ g/mL insulin, 5  $\mu$ g/mL transferrin, 5 ng/mL selenium, and 40 ng/mL dexamethasone. The cells were maintained at 37°C in a 5% (v/v) CO<sub>2</sub> atmosphere and subcultured every 3 days. Transfection with small interfering RNA against the Mettl14 gene (siMettl14: 5'-GCATTGGTGCTGTGT-TAAAdTdT-3') or Hsp90b1 gene (siHsp90b1: 5'-GGA-CATCTCTACAAATTACdTdT-3') was performed. Scrambled small interfering RNA was used as a control.

### Cell Growth/Proliferation and Apoptosis Assays

The cell growth was analyzed by Cell Counting Kit-8 assay following the manufacturer's manuals (cat. CK04; Dojindo, Kumamoto, Japan). Cells were plated in 96-well plates. Solution was added at indicated time points and incubated at 37°C for 1–4 hours. The absorbance at 450 nm

was analyzed. For cell cycle assays, the Cell Cycle Detection Kit (cat. KGA511; KeyGEN BioTECH, Nanjing, China) was used following the instructions. Cells were fixed in cold 75% ethanol overnight, incubated with propidium iodide and RNase A for 30 minutes, and subjected to flow cytometry. For apoptosis assays, the Annexin V-FITC Apoptosis Detection Kit (cat. KGA105; KeyGEN BioTECH) was used following the instructions. Cells were washed by phosphate-buffered saline, stained with Annexin V-FITC and propidium iodide for 5 minutes, and subjected to flow cytometry.

### Statistical Analysis

The data are expressed as means  $\pm$  standard deviation. Statistical comparisons were assessed with Student *t* test with Welch's correction by GraphPad Prism Software 8.0 (San Diego, CA). A *P* value  $<.05$  was considered significant.

### References

1. Taub R. Liver regeneration: from myth to mechanism. *Nat Rev Mol Cell Biol* 2004;5:836–847.
2. Michalopoulos GK. Liver regeneration. *J Cell Physiol* 2007;213:286–300.
3. Kurinna S, Barton MC. Cascades of transcription regulation during liver regeneration. *Int J Biochem Cell Biol* 2011;43:189–197.
4. Michalopoulos GK, Bhushan B. Liver regeneration: biological and pathological mechanisms and implications. *Nature Reviews Gastroenterology & Hepatology* 2021;18:40–55.
5. Forbes SJ, Newsome PN. Liver regeneration: mechanisms and models to clinical application. *Nature Reviews Gastroenterology & Hepatology* 2016;13:473–485.
6. Meyer KD, Jaffrey SR. Rethinking m(6)A readers, writers, and erasers. *Annu Rev Cell Dev Biol* 2017;33:319–342.
7. Fustin JM, Doi M, Yamaguchi Y, Hida H, Nishimura S, Yoshida M, Isagawa T, Morioka MS, Kakeya H, Manabe I, Okamura H. RNA-methylation-dependent RNA processing controls the speed of the circadian clock. *Cell* 2013;155:793–806.
8. Wang X, Lu Z, Gomez A, Hon GC, Yue Y, Han D, Fu Y, Parisien M, Dai Q, Jia G, Ren B, Pan T, He C. N6-methyladenosine-dependent regulation of messenger RNA stability. *Nature* 2014;505:117–120.
9. Wang X, Zhao BS, Roundtree IA, Lu Z, Han D, Ma H, Weng X, Chen K, Shi H, He C. N(6)-methyladenosine modulates messenger RNA translation efficiency. *Cell* 2015;161:1388–1399.
10. Xiao W, Adhikari S, Dahal U, Chen YS, Hao YJ, Sun BF, Sun HY, Li A, Ping XL, Lai WY, Wang X, Ma HL, Huang CM, Yang Y, Huang N, Jiang GB, Wang HL, Zhou Q, Wang XJ, Zhao YL, Yang YG. Nuclear m(6)A reader YTHDC1 regulates mRNA splicing. *Mol Cell* 2016;61:507–519.
11. Meyer KD, Jaffrey SR. The dynamic epitranscriptome: N6-methyladenosine and gene expression control. *Nat Rev Mol Cell Biol* 2014;15:313–326.
12. Liu J, Yue Y, Han D, Wang X, Fu Y, Zhang L, Jia G, Yu M, Lu Z, Deng X, Dai Q, Chen W, He C. A METTL3-METTL14 complex mediates mammalian nuclear RNA N6-adenosine methylation. *Nature Chemical Biology* 2014;10:93–95.
13. Ping XL, Sun BF, Wang L, Xiao W, Yang X, Wang WJ, Adhikari S, Shi Y, Lv Y, Chen YS, Zhao X, Li A, Yang Y, Dahal U, Lou XM, Liu X, Huang J, Yuan WP, Zhu XF, Cheng T, Zhao YL, Wang X, Rendtlew Danielsen JM, Liu F, Yang YG. Mammalian WTAP is a regulatory subunit of the RNA N6-methyladenosine methyltransferase. *Cell Res* 2014;24:177–189.
14. Jia G, Fu Y, Zhao X, Dai Q, Zheng G, Yang Y, Yi C, Lindahl T, Pan T, Yang YG, He C. N6-methyladenosine in nuclear RNA is a major substrate of the obesity-associated FTO. *Nature Chemical Biology* 2011;7:885–887.
15. Zhang C, Samanta D, Lu H, Bullen JW, Zhang H, Chen I, He X, Semenza GL. Hypoxia induces the breast cancer stem cell phenotype by HIF-dependent and ALKBH5-mediated m(6)A-demethylation of NANOG mRNA. *Proc Natl Acad Sci U S A* 2016;113:E2047–E2056.
16. Lin Z, Hsu PJ, Xing X, Fang J, Lu Z, Zou Q, Zhang KJ, Zhang X, Zhou Y, Zhang T, Zhang Y, Song W, Jia G, Yang X, He C, Tong MH. Mettl3-/Mettl14-mediated mRNA N(6)-methyladenosine modulates murine spermatogenesis. *Cell Res* 2017;27:1216–1230.
17. Liu J, Eckert MA, Harada BT, Liu SM, Lu Z, Yu K, Tienda SM, Chryplewicz A, Zhu AC, Yang Y, Huang JT, Chen SM, Xu ZG, Leng XH, Yu XC, Cao J, Zhang Z, Liu J, Lengyel E, He C. m(6)A mRNA methylation regulates AKT activity to promote the proliferation and tumorigenicity of endometrial cancer. *Nat Cell Biol* 2018;20:1074–1083.
18. Wang Y, Li Y, Yue M, Wang J, Kumar S, Wechsler-Reya RJ, Zhang Z, Ogawa Y, Kellis M, Duyster G, Zhao JC. N(6)-methyladenosine RNA modification regulates embryonic neural stem cell self-renewal through histone modifications. *Nat Neurosci* 2018;21:195–206.
19. Weng H, Huang H, Wu H, Qin X, Zhao BS, Dong L, Shi H, Skibbe J, Shen C, Hu C, Sheng Y, Wang Y, Wunderlich M, Zhang B, Dore LC, Su R, Deng X, Ferchen K, Li C, Sun M, Lu Z, Jiang X, Marcucci G, Mulloy JC, Yang J, Qian Z, Wei M, He C, Chen J. METTL14 inhibits hematopoietic stem/progenitor differentiation and promotes leukemogenesis via mRNA m(6)A modification. *Cell Stem Cell* 2018;22:191–205.e199.
20. Chen M, Wei L, Law CT, Tsang FH, Shen J, Cheng CL, Tsang LH, Ho DW, Chiu DK, Lee JM, Wong CC, Ng IO, Wong CM. RNA N6-methyladenosine methyltransferase-like 3 promotes liver cancer progression through YTHDF2-dependent posttranscriptional silencing of SOCS2. *Hepatology* 2018;67:2254–2270.
21. Ma JZ, Yang F, Zhou CC, Liu F, Yuan JH, Wang F, Wang TT, Xu QG, Zhou WP, Sun SH. METTL14 suppresses the metastatic potential of hepatocellular carcinoma by modulating N(6)-methyladenosine-dependent primary microRNA processing. *Hepatology* 2017;65:529–543.
22. Dominissini D, Moshitch-Moshkovitz S, Schwartz S, Salmon-Divon M, Ungar L, Osenberg S, Cesarkas K,

- Jacob-Hirsch J, Amariglio N, Kupiec M, Sorek R, Rechavi G. Topology of the human and mouse m6A RNA methylomes revealed by m6A-seq. *Nature* 2012; 485:201–206.
23. Xia J, Zhou Y, Ji H, Wang Y, Wu Q, Bao J, Ye F, Shi Y, Bu H. Loss of histone deacetylases 1 and 2 in hepatocytes impairs murine liver regeneration through Ki67 depletion. *Hepatology* 2013;58:2089–2098.
24. Walter P, Ron D. The unfolded protein response: from stress pathway to homeostatic regulation. *Science* 2011; 334:1081–1086.
25. Hetz C. The unfolded protein response: controlling cell fate decisions under ER stress and beyond. *Nat Rev Mol Cell Biol* 2012;13:89–102.
26. Argemí J, Kress TR, Chang HCY, Ferrero R, Bértolo C, Moreno H, González-Aparicio M, Uriarte I, Guembe L, Segura V, Hernández-Alcoceba R, Ávila MA, Amati B, Prieto J, Aragón T. X-box binding protein 1 regulates unfolded protein, acute-phase, and DNA damage responses during regeneration of mouse liver. *Gastroenterology* 2017;152:1203–1216.e1215.
27. Liu Y, Shao M, Wu Y, Yan C, Jiang S, Liu J, Dai J, Yang L, Li J, Jia W, Rui L, Liu Y. Role for the endoplasmic reticulum stress sensor IRE1 $\alpha$  in liver regenerative responses. *J Hepatol* 2015;62:590–598.
28. Kim I, Xu W, Reed JC. Cell death and endoplasmic reticulum stress: disease relevance and therapeutic opportunities. *Nature Reviews Drug Discovery* 2008; 7:1013–1030.
29. Szabat M, Page MM, Panzhinskiy E, Skovso S, Mojibian M, Fernandez-Tajes J, Bruin JE, Bround MJ, Lee JT, Xu EE, Taghizadeh F, O'Dwyer S, van de Bunt M, Moon KM, Sinha S, Han J, Fan Y, Lynn FC, Trucco M, Borchers CH, Foster LJ, Nislow C, Kieffer TJ, Johnson JD. Reduced insulin production relieves endoplasmic reticulum stress and induces beta cell proliferation. *Cell Metabolism* 2016;23:179–193.
30. Wu B, Chu X, Feng C, Hou J, Fan H, Liu N, Li C, Kong X, Ye X, Meng S. Heat shock protein gp96 decreases p53 stability by regulating Mdm2 E3 ligase activity in liver cancer. *Cancer Lett* 2015;359:325–334.
31. Sargsyan E, Baryshev M, Szekely L, Sharipo A, Mkrtchian S. Identification of ERp29, an endoplasmic reticulum luminal protein, as a new member of the thyroglobulin folding complex. *J Biol Chem* 2002; 277:17009–17015.
32. Cherepanova N, Shrimal S, Gilmore R. N-linked glycosylation and homeostasis of the endoplasmic reticulum. *Curr Opin Cell Biol* 2016;41:57–65.
33. Xu S, Sankar S, Neamati N. Protein disulfide isomerase: a promising target for cancer therapy. *Drug Discov Today* 2014;19:222–240.
34. Nyfeler B, Reiterer V, Wendeler MW, Stefan E, Zhang B, Michnick SW, Hauri HP. Identification of ERGIC-53 as an intracellular transport receptor of alpha1-antitrypsin. *J Cell Biol* 2008;180:705–712.
35. Chen CY, Ezzeddine N, Shyu AB. Messenger RNA half-life measurements in mammalian cells. *Methods Enzymol* 2008;448:335–357.
36. Rachidi S, Sun S, Wu BX, Jones E, Drake RR, Ogretmen B, Cowart LA, Clarke CJ, Hannun YA, Chiosis G, Liu B, Li Z. Endoplasmic reticulum heat shock protein gp96 maintains liver homeostasis and promotes hepatocellular carcinogenesis. *J Hepatol* 2015; 62:879–888.
37. Hamano M, Ezaki H, Kiso S, Furuta K, Egawa M, Kizu T, Chatani N, Kamada Y, Yoshida Y, Takehara T. Lipid overloading during liver regeneration causes delayed hepatocyte DNA replication by increasing ER stress in mice with simple hepatic steatosis. *J Gastroenterol* 2014; 49:305–316.
38. Lu XF, Cao XY, Zhu YJ, Wu ZR, Zhuang X, Shao MY, Xu Q, Zhou YJ, Ji HJ, Lu QR, Shi YJ, Zeng Y, Bu H. Histone deacetylase 3 promotes liver regeneration and liver cancer cells proliferation through signal transducer and activator of transcription 3 signaling pathway. *Cell Death Dis* 2018; 9:398.
39. Wang S, Zhang C, Hasson D, Desai A, SenBanerjee S, Magnani E, Ukomadu C, Lujambio A, Bernstein E, Sadler KC. Epigenetic compensation promotes liver regeneration. *Dev Cell* 2019;50:43–56.e46.
40. Zhou Y, Zhang L, Ji H, Lu X, Xia J, Li L, Chen F, Bu H, Shi Y. MiR-17~92 ablation impairs liver regeneration in an estrogen-dependent manner. *J Cell Mol Med* 2016; 20:939–948.
41. Geula S, Moshitch-Moshkovitz S, Dominissini D, Mansour AA, Kol N, Salmon-Divon M, Hershkovitz V, Peer E, Mor N, Manor YS, Ben-Haim MS, Eyal E, Yunger S, Pinto Y, Jaitin DA, Viukov S, Rais Y, Krupalnik V, Chomsky E, Zerbib M, Maza I, Rechavi Y, Massarwa R, Hanna S, Amit I, Levanon EY, Amariglio N, Stern-Ginossar N, Novershtern N, Rechavi G, Hanna JH. Stem cells: m6A mRNA methylation facilitates resolution of naive pluripotency toward differentiation. *Science* 2015;347:1002–1006.
42. Wang Y, Li Y, Toth JI, Petroski MD, Zhang Z, Zhao JC. N6-methyladenosine modification destabilizes developmental regulators in embryonic stem cells. *Nat Cell Biol* 2014;16:191–198.
43. Lee H, Bao S, Qian Y, Geula S, Leslie J, Zhang C, Hanna JH, Ding L. Stage-specific requirement for Mettl3-dependent m(6)A mRNA methylation during haematopoietic stem cell differentiation. *Nat Cell Biol* 2019; 21:700–709.
44. Huang H, Weng H, Zhou K, Wu T, Zhao BS, Sun M, Chen Z, Deng X, Xiao G, Auer F, Klemm L, Wu H, Zuo Z, Qin X, Dong Y, Zhou Y, Qin H, Tao S, Du J, Liu J, Lu Z, Yin H, Mesquita A, Yuan CL, Hu YC, Sun W, Su R, Dong L, Shen C, Li C, Qing Y, Jiang X, Wu X, Sun M, Guan JL, Qu L, Wei M, Muschen M, Huang G, He C, Yang J, Chen J. Histone H3 trimethylation at lysine 36 guides m(6)A RNA modification co-transcriptionally. *Nature* 2019;567:414–419.
45. Wang GL, Iakova P, Wilde M, Awad S, Timchenko NA. Liver tumors escape negative control of proliferation via PI3K/Akt-mediated block of C/EBP alpha growth inhibitory activity. *Genes Dev* 2004;18:912–925.

46. Johnson PF. Molecular stop signs: regulation of cell-cycle arrest by C/EBP transcription factors. *J Cell Sci* 2005;118(Pt 12):2545–2555.
47. Yong J, Itkin-Ansari P, Kaufman RJ. When less is better: ER stress and beta cell proliferation. *Dev Cell* 2016; 36:4–6.

---

Received October 26, 2020. Accepted April 1, 2021.

#### Correspondence

Address correspondence to: Yujun Shi, PhD, MD, Laboratory of Pathology, West China Hospital, Sichuan University, 37 Guoxue Road, Chengdu 610041, China. e-mail: [shiyujun@scu.edu.cn](mailto:shiyujun@scu.edu.cn); fax: +86-028-85164030 or Chuan Li, PhD, MD, Department of Liver Surgery, West China Hospital, Sichuan University, Chengdu 610041, China. e-mail: [lichuan85@163.com](mailto:lichuan85@163.com); fax: +86-028-85422871 or Yuping Gong, PhD, MD, Department of Hematology, West China Hospital, Sichuan University, Chengdu 610041, China. e-mail: [gongyuping@hotmail.com](mailto:gongyuping@hotmail.com); fax: +86-028-85423351.

#### Acknowledgments

The authors thank Dr Ming-Han Tong for providing transgenic mice and also thank Li Li and Fei Chen for pathology technique assistance.

#### CRediT Authorship Contributions

Xiaoyue Cao (Conceptualization: Supporting; Data curation: Lead; Formal analysis: Lead; Methodology: Lead; Writing – original draft: Lead)  
 Yuke Shu (Data curation: Supporting; Formal analysis: Supporting; Methodology: Supporting)  
 Yuwei Chen (Data curation: Supporting; Methodology: Supporting)  
 Qing Xu (Methodology: Supporting)  
 Gang Guo (Formal analysis: Supporting; Writing – review & editing: Supporting)  
 Zhenru Wu (Methodology: Supporting)  
 Mingyang Shao (Formal analysis: Supporting; Software: Supporting)  
 Yongjie Zhou (Conceptualization: Supporting; Software: Supporting)  
 Menglin Chen (Methodology: Supporting)  
 Yuping Gong (Writing – review & editing: Supporting)  
 Chuan Li (Funding acquisition: Supporting; Writing – review & editing: Supporting)  
 Yujun Shi (Conceptualization: Lead; Supervision: Lead; Writing – review & editing: Lead)  
 Hong Bu (Writing – review & editing: Supporting)

#### Conflicts of interest

The authors disclose no conflicts.

#### Funding

Supported by grants from the Natural Science Foundation of China (No. 81900576) and 1.3.5 Project for Disciplines of Excellence, West China Hospital, Sichuan University (2020HXFH010 and ZYJC18008).